Biomarker and pollen evidence for late Pleistocene pluvials in the Mojave Desert

Mark D. Peaple[1], Tripti Bhattacharya[2], Tim K. Lowenstein[3], David McGee[4], Kristian J. Olson[3], Justin S. Stroup[5], Jessica E. Tierney[6], Sarah J. Feakins[1]

[1]Department of Earth Sciences, University of Southern California, Los Angeles, CA 90089

[2]Department of Earth and Environmental Sciences, Syracuse University, Syracuse NY 13210

[3]Department of Geological Sciences and Environmental Studies, State University of New York, Binghamton, New York 13902, USA

[4]Department of Earth, Atmospheric and Planetary Sciences, Massachusetts Institute of Technology, Cambridge, MA 02139

[5]Department of Atmospheric and Geological Sciences, State University of New York at Oswego, Oswego, NY 13126

[6]Department of Geosciences, University of Arizona, Tucson, AZ 85721

Key points

- Biomarker and pollen record from Searles Lake, CA sediment core spanning 200 kyr
- Changes in plant wax hydrogen isotopes consistent with regional speleothems
- Archaeal lipids reveal lake highstands, Termination 2 wetter than Termination 1

Abstract

The climate of the southwestern North America has experienced profound changes between wet and dry phases over the past 200 kyr. To better constrain the timing, magnitude and paleoenvironmental impacts of these changes in hydroclimate, we conducted a multiproxy biomarker study from samples collected from a new 76 m sediment core (SLAPP-SRLS17) drilled in Searles Lake, California. Here, we use biomarkers and pollen to reconstruct vegetation, lake conditions and climate. We find that δD values of long chain *n*-alkanes are dominated by glacial to interglacial changes that match nearby Devils Hole calcite $\delta^{18}O$ variability, suggesting both archives predominantly reflect precipitation isotopes. However, precipitation isotopes do not simply covary with evidence for wet-dry changes in vegetation

and lake conditions, indicating a partial disconnect between large scale atmospheric circulation tracked by precipitation isotopes and landscape moisture availability. Increased crenarchaeol production and decreased evidence for methane cycling reveal a 10 kyr interval of a fresh, productive and well-mixed lake during Termination II, corroborating evidence for a paleolake highstand from shorelines and spillover deposits in downstream Panamint Basin during the end of the penultimate (Tahoe) glacial (140–130 ka). At the same time brGDGTs yield the lowest temperature estimates (mean months above freezing = 9 ± 3°C) of the 200 kyr record. These limnological conditions are not replicated elsewhere in the 200 kyr record, suggesting that the Heinrich stadial 11 highstand was wetter than that during the last glacial maximum and Heinrich 1 (18–15 ka).

Keywords: plant wax; GDGTs; hydrogen isotopes; carbon isotopes; pollen

Plain language summary

Searles Valley in the Mojave Desert, California, contains a saltpan, the remnants of a former lake. Shoreline features show the former lake was at times 274 m deep. We studied the ancient lake mud and salt deposits below the valley floor to a depth of 76 m, in a sediment core drilled in 2017. The remains of microbes and plants allow us to reconstruct past climate conditions. We find that during cooler glacial periods, conifer forests covered the landscape and plant wax in the core records rainfall that is chemically different to today. These differences are similarly recorded in nearby cave deposits, suggesting changing storm tracks. The wettest climates were found in the cool climate of the penultimate glacial (about 135 000 years ago), when Searles Lake vigorously overflowed into Panamint Basin.

1. Introduction

There is considerable concern over water availability in southwestern North America and

uncertainties around precipitation in climate model projections (Pierce et al., 2013). Proxy reconstructions of past moisture availability under different temperature regimes can help to understand the changing water balance (P–E) during periods of climate change (David McGee, 2020), including evidence for water table rise and fall in the southwestern North America detected during recent glacial cycles (Wendt et al., 2018).

However, available proxy evidence from southwestern North America suggests different magnitudes of variability and climate change during the late Pleistocene. For instance, Devils Hole and the Leviathan composite record (Figure 1a) are high resolution speleothem $\delta^{18}O$ records which record glacial interglacial changes in $\delta^{18}O$ of precipitation over two glacial cycles (M. S. Lachniet, 2016; Moseley et al., 2016). However, the magnitudes of variability are larger and precessional pacing is more strongly represented in the Leviathan composite record than in the Devils Hole calcite. It is likely that differences in aquifer mixing, karstic dissolution and calcite precipitation processes (including temperature) lead to differences between $\delta^{18}O_{calcite}$ in the different cave systems and speleothem types. Independent evidence for precipitation isotopic composition for the last glacial is available from groundwater, studied further south in San Diego, but only for the last glacial (Kulongoski et al., 2009; Seltzer et al., 2021). Lake sediments provide a longer archive of precipitation isotopes, for example, the plant wax δD record back to 33 ka from Lake Elsinore, California (Figure 1a) (Feakins et al., 2019). Biomarker studies of Lake Elsinore sediments, specifically bacterial membrane lipids, also yielded evidence of previously unrecognized, highly-variable lake temperatures during the last glacial period (Feakins et al., 2019). Fossil pollen in sediment cores from Lake Elsinore and Searles Lake provide evidence for past vegetation and yield insights into past hydroclimate (Heusser et al., 2015; Litwin et al., 1999). However, vegetation composition can be influenced by multiple variables (e.g., temperature, pCO_2, and

rainfall).

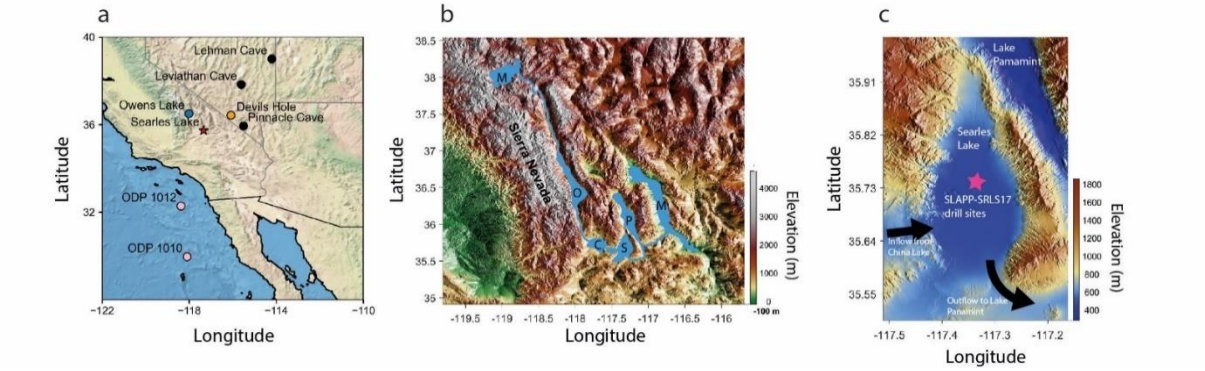

Figure 1. Maps showing location of A) Searles Lake (red star) and climate archives referred to in the text including Owens Lake (blue circle), ODP 1012/1010 (pink circles), Devils Hole (orange circle), Leviathan Cave, Lehman Cave, and Pinnacle Cave (black circles) B) The Lakes connected to Searles Lake during pluvial periods where M = Mono Lake, O = Owens Lake, C = China Lake, S = Searles Lake, P = Lake Panamint, M = Lake Manly. C) Map of Searles Lake under during pluvial conditions highlighting inflow and outflow.

Here we revisit lacustrine sediments from Searles Lake (Figure 1c), to generate a 200 kyr biomarker and pollen reconstruction of limnology as well as regional climate and environmental changes. The combination of plant wax and pollen allows us to independently infer changes in regional precipitation δD and vegetation, which act as tracers for changes in rainfall seasonality in this region. In addition, we analyze a suite of microbial biomarkers to reconstruct aridity and inform on lake salinity, depth, and temperature. The multi-proxy dataset uniquely yields new insights into the timing and magnitude of past changes between aridity and pluvials that filled the chain of lakes to the east of the Sierra Nevada Mountains (Figure 1b) in what is today part of the hyperarid Mojave Desert.

1.1. Regional setting

Searles Valley is an endorheic basin located in the Mojave Desert in southeastern California (Figure 1). Below the evaporites on the valley floor, there are lacustrine muds from past deep

lake conditions. Shoreline tufa deposits indicate the lake was formerly up to ~300 m deep (Smith et al., 1983). During past wet climate states, the Owens River carried spill-over from the upstream Owens Lake to China Lake and Searles Lake (Figure 1c). Owens Lake receives snowmelt runoff from the eastern flanks of the Sierra Nevada Mountains (Bischoff & Cummins, 2001). Over the past 200 ka, the Owens River has been almost continuously inflowing into Searles Lake, with only the late Holocene and 6 brief (<1 ka) periods during the late glacial receiving no inflow (Bacon et al., 2020). Once between 190 and 130 ka, the catchment may have briefly expanded to include that of Mono Lake (Reheis et al., 2002). When Searles Lake reached 696 m, it would also reach the spillway into Panamint Basin and ultimately Death Valley (Forester et al., 2005).

The present-day climate in Searles Valley is hyperarid, with a mean annual precipitation of 100 mm between 1920 – 2016 (Western Regional Climate Center, 2022). Modern monthly mean temperature averages 27.4°C in summer (JJA) and 11.4°C in winter (DJF) with recorded temperature extremes of 41.0°C and -0.8°C (Western Regional Climate Center, 2022). Hot, dry, and often windy, conditions promote high potential evaporation ~2000 mm/yr, far in excess of precipitation. Sporadic precipitation is winter-dominated with DJF and JAS monthly means of 18 mm and 4 mm respectively (Western Regional Climate Center, 2022). During past pluvial conditions, Searles would receive precipitation falling on the Eastern Sierra Nevada Mountains through Owens River inflow. Modern Eastern Sierra precipitation also has a winter dominance with DJF and JAS monthly means of 67 mm and 16 mm respectively (Lake Sabrina) (Western Regional Climate Center, 2022). Local winter precipitation is sourced from storms that derive from the North Pacific in addition to sub-tropical sourced atmospheric rivers (Friedman et al., 1992). Summer rain is sourced from the Gulf of California and Gulf of Mexico at the northern limits of incursion of the North

American Monsoon, with a small contribution from North Pacific moisture (Friedman et al., 1992). Precipitation from northerly winter and summer storms is typically more D-depleted than southerly sourced moisture in either winter or summer (Friedman et al., 2002), with Searles Valley precipitation having mean summer (March to September) and winter (October to April) δD values of -56‰ and -76‰ respectively (collection dates 1982–1989, Friedman et al., 1992). Measured winter precipitation in Owens Valley is more D-depleted (mean October to April = –96‰) than in Searles Valley (mean October to April = –74‰) due to Rayleigh distillation in rainout over the Sierra Nevada topographic barrier (~4 km). Additionally, moisture can leak to the south of the mountain range across the Mojave Desert (Friedman et al., 1992) and can become enriched by evaporation during raindrop descent (Friedman et al., 2002). Summer precipitation isotopic compositions reported from Searles Valley (mean, –57‰) and Owens Valley (mean, –62‰) are similar (Friedman et al., 1992). The relative enrichment of summer rainfall could reflect a greater proportion of convective rainfall in summer in addition to the re-evaporation of raindrops as they fall in a hot, low humidity environment (Friedman et al., 1992; Berkelhammer et al., 2012).

1.2. Age Model

Sediment cores SLAPP-SRLS17-1A and 1B (35.7372ºN, 117.33ºW, 495 m asl) were drilled from Searles Lake in 2017 with 95% recovery extending to 78 m below lake floor (Figure 1b). U/Th dating of evaporite minerals (Stroup et al., in prep), indicate the recovered sediments span 200 ka BP. Stroup et al., (in prep) use 37 U-Th ages to construct a Bayesian age model using BACON. The model takes into consideration the mineralogy, stratigraphic superposition, and boundaries between lithological units. To constrain a portion of the mud horizons without salt minerals suitable for dating, a tie point near Termination 2 (T2) was

identified linking the δD_{31alk} record (generated in this study) to the Leviathan composite record $\delta^{18}O_{calcite}$ record, following the approach of Wang et al., (2022). The data were scaled and interpolated before applying a low pass filter to both records to remove high frequency variability. We then calculated the second derivatives to identify a match point at a gradient of 0. An age constraint of 126.5 ± 0.5 ka from the Leviathan composite record was applied to the feature found at 54.5 m depth in SLAPP-SRLS17-1A. This tie point assumes that changes in the speleothem $\delta^{18}O$ in Nevada and leaf wax δ D in Searles Basin should closely correspond with each other; this assumption is supported by the good agreement between regional speleothem records and Searles basin δD_{wax} over the last 100 ka, when the records are anchored by independent U-Th-based age models (section 3.2). Between 200–50 ka the accumulation rate of lacustrine carbonate muds was 0.2 m/ka (95% CI, ± 3.5 ka). After 50 ka sediments and salts accumulated more rapidly (1.3 m/ka). The late glacial and deglacial age model is well constrained (± 0.9 ka), but the late Holocene is less well resolved due to slowed deposition since the lake desiccated completely and mining disturbed the record in the upper salts.

2. Material and methods

2.1. Lipid extraction

Lacustrine muds were sampled in 2018 for biomarkers and pollen roughly every 60 cm (~2 ka), avoiding salts that dominate the upper 33 m of the core. As previously described in Peaple et al. (2021), 120 sediment samples (~20 g) were dried, ground and extracted using a Dionex Accelerated Solvent Extraction system at the University of Southern California with 9:1 dichloromethane (DCM):methanol (MeOH) at 100ºC and 1500 psi to yield the Total Lipid Extract (TLE). Briefly, the TLEs were separated into neutral and acid fractions by

column chromatography. The neutral fraction was further separated using columns packed with 5% deactivated silica gel, eluting *n*-alkanes with hexanes and the polar fraction with DCM followed by methanol. *n*-Alkanes were treated with copper to remove elemental sulfur prior to GC analyses. Fatty acids were methylated (to FAMEs) using 95:5 MeOH:hydrochloric acid, at 70ºC for 12 h, using MeOH of known isotopic composition (methyl group $\delta^{13}C$ of –24.7‰ and δD of –187‰).

2.2. GDGT analyses

The neutral polar fraction was analyzed by an Agilent 1260 High-Performance Liquid Chromatography (HPLC) coupled to an Agilent 6120 mass spectrometer at the University of Arizona, following the methods of Hopmans et al. (2016). Compounds were detected in single ion monitoring mode and quantified relative to a C_{46} internal standard. Concentrations of archaeol, caldarchaeol and the ACE index for salinity were previously reported (Peaple et al., 2021). Here we report concentrations of individual and summed (Σ) isoGDGTs and brGDGTs and calculate temperature, pH and methane sensitive indicators.

We calculate the branched isoprenoid tetraether (BIT) index:

$$BIT = \frac{Ia+IIa+IIa'+IIIa+IIIa'}{Ia+IIa+IIa'+IIIa+IIIa'+cren} \quad (1)$$

where brGDGTs Ia IIa and IIIa, including both the 5´ and 6´ methyl isomers, are compared with the abundance of crenarchaeol (Hopmans et al., 2004). In lakes BIT has traditionally been interpreted to be represent the balance between soil inputs of brGDGTs and lake production of crenarchaeol (e.g. Verschuren et al., 2009). However interpretations may differ as bacterial production may dominate in many lakes, and changes in oxycline depth may control the abundance of creanarchaeol-producing Thaumarchaeota (Baxter et al., 2021). As

an additional measure of stratification, we calculate %GDGT-0 (Sinninghe Damsté, Ossebaar, et al., 2012) which measures the proportion of isoGDGT-0, which is produced by Thaumarcheota (e.g. Sinninghe Damsté et al., 2012b; Schouten et al., 2013), anaerobic methane-oxidizing archaea (Pancost et al., 2001; Schouten et al., 2001) and methanogenic Euryarchaeota (Schouten et al., 2013, and references therein) relative to crenarchaeol which is produced uniquely by Thaumarchaeota (e.g. Sinninghe Damsté et al., 2002; Schouten et al., 2013) :

$$\%\mathrm{GDGT}-0=\frac{[GDGT-0]}{[GDGT-0]+[\mathrm{Crenarchaeol}]}\times 100 \quad (2)$$

We calculate the CBT′ index (De Jonge et al., 2014) where:

$$CBT'=log_{10}\left[\frac{Ic+IIa'+IIb'+IIc'+IIIa'+IIIb'+IIIc'}{Ia+IIa+IIIa}\right] \quad (3)$$

CBT′ has been calibrated to pH in east African lakes (Russell et al., 2018):

$$pH=7.15-1.59*CBT' \quad (4)$$

The temperature sensitive MBT'_{5Me} index is the relative methylation of the 5′ isomers of the brGDGTs (De Jonge et al., 2014, Hopmans et al., 2016), is expressed as:

$$MBT'_{5ME}=\frac{(Ia+Ib+Ic)}{(Ia+Ib+Ic+IIa+IIb+IIc+IIIa)} \quad (5)$$

where the Type I, II and III brGDGTs have four, five, and six methyl groups respectively and the Type a, b, and c brGDGTs has zero, one, and two rings, respectively. Duplicate analyses as well as analyses of an internal laboratory standard throughout the runs yielded an error of 0.009 MBT'_{5Me} units (1σ). To convert MBT'_{5Me} to temperature we use the Bayesian $BayMBT_0$ model which was generated by calibrating MBT'_{5Me} against the mean temperature of the months above freezing from a global lake dataset (Martínez-Sosa et al., 2021),

including lakes over a range of pH (4.3 to 10), salinity (0–275 psu) and temperature (1.6 to 28.1°C).

We calculate IR_{6+7Me}, an index sensitive to changes in lake salinity (H. Wang et al., 2021):

$$IR_{6+7Me} = \left[\frac{IIa'+IIb'+IIc'+IIIa'+IIIb'+IIIc'}{IIa+IIb+IIc+IIIa+IIIb+IIIc+IIa'+IIb'+IIc'+IIIa'+IIIb'+IIIc'} + \frac{IIIa'''+IIa'''}{IIIa+IIIa'+IIIa'''+IIa+IIa'+IIa'''}\right] \times 0.5 \quad (6)$$

We also calculate TEX_{86} for all samples (Schouten et al., 2002):

$$TEX_{86} = \frac{([GDGT-2]+[GDGT-3]+[cren\prime])}{([GDGT-1]+[GDGT-2]+[GDGT-3]+[cren\prime])} \quad (7)$$

and convert to lake surface temperature (LST) using the calibration (Tierney et al., 2010):

$$LST = TEX_{86} \times 38.874 - 3.4992 \quad (8)$$

in a single sample where BIT <0.3 and %GDGT-0 <50 indicating high thaumarcheotal relative abundance.

2.3. Compound specific isotopic analyses

n-Alkanoic acids and *n*-alkanes were identified using an Agilent 6890 Gas Chromatograph (GC) connected to an Agilent 5973 MSD mass spectrometer (MS), and quantified by flame ionization detector (FID). Abundances, average chain length (ACL) and carbon preference index (CPI) were previously reported in (Peaple et al., 2021). The carbon and hydrogen isotopic composition of *n*-alkanoic acids and *n*-alkanes were measured for this study using a Thermo Scientific Trace GC equipped with a Rxi®–5 ms column (30 m × 0.25 mm, film thickness 0.25 μm) with a PTV injector in solvent-split mode, coupled via an Isolink combustion/pyrolysis furnace (1000/1400°C) to a Thermo Scientific Delta V Plus isotope ratio mass spectrometer (IRMS) at the University of Southern California. Reference gas

linearity was assessed daily across 1–8 V, for $\delta^{13}C$ ($1\sigma = 0.04‰$), and for δD (H_3^+ factor = 10.6 ppm/mV). A standard containing C_{16}-C_{30} *n*-alkanes of known isotopic compositions (A6 mix supplied by A. Schimmelmann, University of Indiana; $\delta^{13}C$ values from –25.9 to –33.7‰ and δD values from –17 to –256‰) was measured daily, allowing for normalization to Vienna Standard Mean Ocean Water (VSMOW) and Vienna Pee Dee Belemnite (VPDB) respectively. Reported $\delta^{13}C$ and δD values for *n*-alkanoic acids were corrected to account for the contribution of the methyl group.

2.4. Palynological Analyses

Pollen assemblages were studied for 113 samples at Syracuse University; for detailed sample processing methodology see the Supplementary Information. Pollen samples were counted on 400x and 1000x magnification, and compared to known pollen keys (Kapp et al., 2000). Our counts found 22 unique taxa, though samples were dominated by *Pinus* pollen (e.g. greater than 40% of each sample). Pollen assemblages are expressed in percentages as well as pollen influx rates (grains/cm^2/yr). The similarity of the broad trends across these two ways of expressing the pollen data increases our confidence that the patterns in our data are robust. For our analysis, we exclude one sample at 27.49 m that was associated with a tephra layer. To identify the patterns of variability in the pollen data, we calculated the Bray-Curtis dissimilarity index between samples, using pollen taxa that were present in 2 or more samples at a percentage of greater than 2%. This index calculates the compositional dissimilarity between two ecological samples in space or time, and minimizes the contribution of rare taxa to dissimilarity between samples (Faith et al., 1987). We used a matrix of pairwise Bray-Curtis indices between all samples to perform a non-metric multidimensional scaling (NMDS). NMDS iteratively moves all samples in 2-dimensional ordination space so that their final distance from each pairwise sample is proportional to the Bray-Curtis dissimilarity

between those two samples. It is analogous to principle components analysis in that the distance between samples on the plot provides a guide to their dissimilarity, but is more robust for assemblages containing rare taxa (Faith et al., 1987; Fasham, 1977). The results from this NMDS analysis are used to guide our interpretation of specific plant taxa in the pollen record.

2.5. Correlation analysis

All correlations between time series use non-parametric methods that account for serial correlation (Ebisuzaki, 1997).

3. Results and Discussion

3.1. Vegetation reconstructions from Searles Lake spanning 200 kyr

We present a multi-proxy biomarker and pollen study of vegetation change as recovered from the sediments of Searles Lake in the SLAPP-SRLS17 sediment core. All vegetation-related data obtained from the core are shown in stratigraphic context (Figure S4) and on the age scale (Figure 2). Pollen reconstructions are dominated by Pinus (Figure 2), because of their long pollen dispersal distances and high pollen production (Campbell et al., 1999; Wood, 2000). The Owens Lake pollen record suggests that during glacials pines may have expanded into lowlands while being restricted in the uplands (Litwin et al., 1999; Woolfenden, 2003). Pollen from other taxa can offer more diagnostic climatic information: during cooler/wetter glacial periods Taxodiaceae-Cupressaceae-Taxaceae (TCT), mostly Juniper, increase. Elsewhere, glacial increases in Juniperus-type pollen have been noted from the Gulf of California to the Great Basin (Byrne, 1982; Davis, 1998). Packrat middens confirm this expansion across the southwestern North America at the LGM (Koehler et al., 2005; Thompson & Anderson, 2000). Middens in the Central Mojave specifically identify the glacial expansion of *J. osteosperma*, which is more sensitive to water stress than other taxa in

279 this genus, e.g., *J. californica* (Holmgren et al., 2010; Koehler et al., 2005; Willson et al.,
280 2008) indicating more moisture availability in the lowlands. During interglacials, Juniper
281 declined and herbaceous taxa like Asteraceae and Amaranthaceae increased in the Searles
282 basin (Figure 2a). We sum the representation of Asteraceae and Amaranthaceae together to
283 represent the total number of desert shrubs in the record. NMDS analysis reveals that glacial
284 and interglacial samples from Searles lake show distinct pollen assemblages, and that these
285 changes are primarily driven by changing proportions of desert shrub pollen, as well as
286 *Juniperus*-type pollen (Figure S4). Desert shrub proportions were previously modeled by
287 machine learning on *n*-alkane and *n*-alkanoic acid homologs in the same sediments (Peaple et
288 al., 2021; Figure. 2b), and the comparison with desert shrubs reconstructed by pollen (Figure.
289 2c) indicates similar long-term trends when high frequency changes are removed ($r = 0.42$,
290 $p>0.01$). Pollen aids paleovegetation interpretations as it reveals the specific plant taxa
291 present, but it does not inform on plant wax sourcing since pollen and waxes may have
292 distinct transport mechanisms to the lake basin. For example, Juniper produce a distinct
293 molecular abundance distribution, with modal C_{33} *n*-alkanes (Diefendorf et al., 2015), but we
294 find this compound is not abundant in Searles Lake sediments even during glacials, when
295 pollen and packrat midden macrobotanicals show that they thrived.

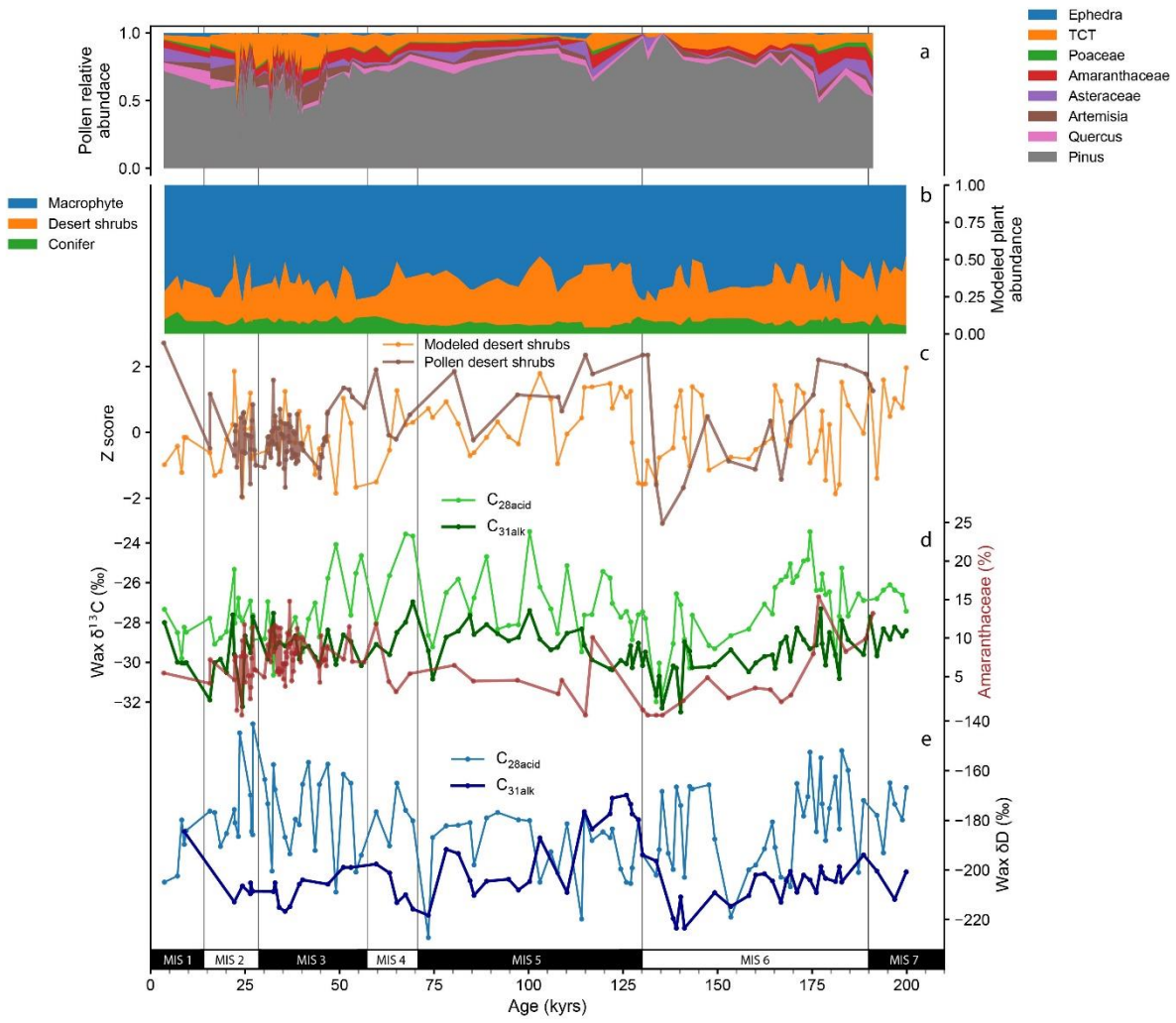

Figure 2. Vegetation reconstructions using pollen and plant wax proxies from SLAPP-SRLS17. A) Proportion of pollen taxa. B) Modelled vegetation types based on SVM machine learning of plant wax distributions in modern taxa applied to the downcore record (Peaple et al., 2021). C) Comparison between modelled desert plant types and pollen "desert shrubs" (the sum of Amaranth and Asteraceae pollen). D) $\delta^{13}C_{28acid}$ and $\delta^{13}C_{31alk}$ compared to Amaranth pollen. E) δD_{28acid} and δD_{31alk}.

Pollen microfossil assemblages were analyzed in different core samples than the biomarkers so each were linearly interpolated onto 2 kyr sampling resolution to assess shared variance by principal component analysis (PCA; Figure 3). The PCA analysis identifies a negative relationship between dominant pine pollen and TCT (*Taxodiaceae-Cupressaceae-Taxaceae*, in this case mostly *Juniperus* spp.). Juniper is associated with Artemisia, denoting their

glacial co-occurrence (Figures 2 and 3). The ACE salinity index and desert taxa *Amaranthaceae* show a correspondence between lake salinity and desert plants, similar to their association on salty lowland areas of the valley today. Shrub pollen increases with warming, consistent with prior reports that shrub vegetation is temperature responsive (Lyle et al., 2010).

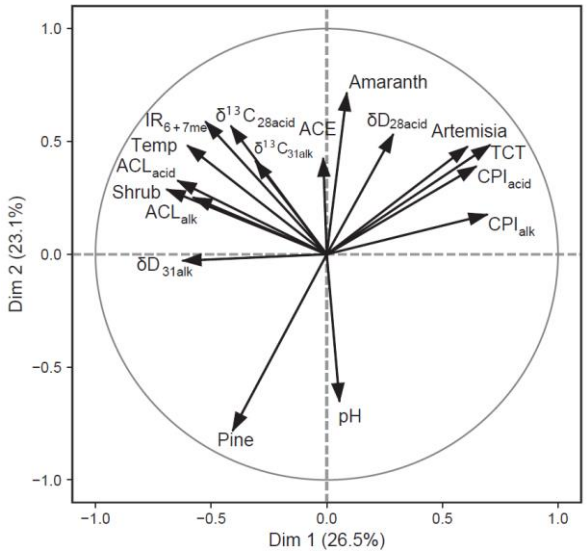

Figure 3. PCA to assess biomarker and pollen covariations (Shrub = sum of Amaranthaceae and Asteraceae pollen abundance).

Carbon isotope evidence from plant wax biomarkers reveals additional information about vegetation. The $\delta^{13}C_{31alk}$ and $\delta^{13}C_{28acid}$ covary (Figure 3), although the range of values differ (Figure 2), reflecting similar pacing but potentially differences in sourcing, with C_{31alk} broadly reflecting terrestrial plants and C_{28acid} reflecting conifers and/or aquatic inputs. $\delta^{13}C$ increases under warmer conditions, as shown through similar correlations with PC 1 and 2 (Figure 2), likely driven by increasing water stress on C_3 plants. $\delta^{13}C$ also increases with higher Amaranthaceae (C_4 and C_3 members) pollen percentages as well as influx rates (Figures 2d, 3 and Figure S4), which suggests that temperature controlled evaporative demand, rather than pCO_2, is the dominant selection pressure on the prevalence of C_4 woody

taxa in this region. In contrast, grasses are nearly absent from the pollen record during interglacial intervals, making it unlikely that the $\delta^{13}C$ signal reflects C_4 grasses (Figure 2a). The C_4 pathway is used in some woody, halophilic desert plants sampled in the catchment today, including plants in the *Atriplex* and *Suaeda* genera. These plants are phreatophytes, and thrive in locations with shallow groundwater (Patten et al., 2008). Warmer temperatures may drive the expansion of these taxa by increasing the area of seasonal environments C_4 Amaranthaceae taxa occupy. Warmer conditions would likely also restrict the habitat of drought-sensitive *Juniperus* species and promote the expansion of conifer-dominated environments (Figure 2).

The lack of correlation between the δD_{28acid} and δD_{31alk} indicates a difference in the signals captured by these two compound classes in Searles Lake. The δD_{28acid} is puzzling as it records D-enrichment during glacials, opposite to hydroclimate expectations, suggesting producer complications. δD_{28acid} anticorrelates with pines (Figure 3), likely reflecting their abundant production of fatty acids. During the LGM (locally termed the Tioga glaciation), the upper limit of tree production descended from 3.5 to to 2.5 km as glaciers and snowpack accumulated (Moore & Moring, 2013). The elimination of the highest elevation conifer forests during glacials could increase the δD value of exported plant wax *n*-alkanoic acids by at most 10‰ based on the expected altitude effect (Feakins et al., 2018). A glacial expansion of lowland conifers could further add D-enriched lowland production. However, it seems unlikely the altitude source effect could explain all of the 40‰ variability observed downcore (Figure 2e). Machine learning has suggested the possibility of aquatic macrophyte inputs (Peaple et al., 2021), although unverified locally, given the lack of modern surface water. There is some upstream macrophyte evidence from palynology of Owens Lake (Woolfenden, 2003), although none in Searles Lake (this study). The δD signal of aquatic production

(whether by macrophytes or microbial production) would be affected by changing lake water δD as well as lake salinity effects on fractionation (Sachse et al., 2012). Rather than attempt to further theorize about multiple unknowns, we suggest that both upland conifer and aquatic production may produce complications, confounding the δD_{28acid} signal here.

In contrast the *n*-alkanes yield a clear D-depleted glacial and D-enriched interglacial pattern (Figure 2e). δD_{31alk} has a close phasing with desert shrub pollen (sum of *Amaranthaceae* and *Asteraceae*) and temperature (Figures 2c and 3) and this covariation of proxies suggests a common driver which will be explored when compared to regional and global climate (in Section 4.2). During arid climates, like today, we assume that desert shrubs dominate the *n*-alkane record. Although the details are necessarily unconstrained for past pluvial climates in southern California, trees in modern temperate North American forests and woodlands are prolific producers of *n*-alkanes and have been shown to contribute strongly to lakes rather than the marginal plants (Freimuth et al., 2019). We thus infer that plant wax *n*-alkanes may have been supplied by wind transport to Searles Lake from the woody shrubs and trees of the surrounding lowlands. We reconstruct δD_{precip} using the local constant fractionation by plants ($\varepsilon_{31alk/p,}$ -93‰), determined from regional calibration across the modern aridity gradient (Feakins and Sessions, 2010). Sensitivity tests that assess the effect of changing vegetation based on pollen and plant wax $\delta^{13}C$ (Figure S2) lead to confidence in the constant fractionation and hydroclimate interpretations here. Climate model experiments support theoretical expectations of D-depletion associated with condensation at colder temperatures and as ice versus liquid cloud droplets and as would be expected in a glacial climate (Jasechko et al., 2015) together with changing storm tracks introducing more D-depleted North Pacific sourced moisture (Oster et al., 2015) and a decrease in enriched North

374 American Monsoon sourced precipitation (Bhattacharya et al., 2018).

375 **3.2. Plant wax evidence for glacially paced changes in hydroclimate**

376 The Searles Lake δD_{31alk} record (Figure 4) is dominated by glacial to interglacial variability,
377 with interglacials characterized by more positive values and glacials by more negative values.
378 After accounting for the ice volume corrections for seawater δD, and the apparent
379 fractionation by plants, we can interpret plant wax δD_{31alk} as precipitation isotopic variations
380 (Figure 4c, see Supplemental Information for method details). δD_{precip} during interglacials
381 averages –87‰ and during glacials averages –127‰. The Searles δD_{precip} closely matches
382 global climate records of glacial to interglacial changes in pCO_2 (Figure 4b), ice volume, and
383 deep ocean temperature changes interpreted from benthic foraminiferal oxygen isotopes
384 (Figure 4c) across two glacial-interglacial cycles.

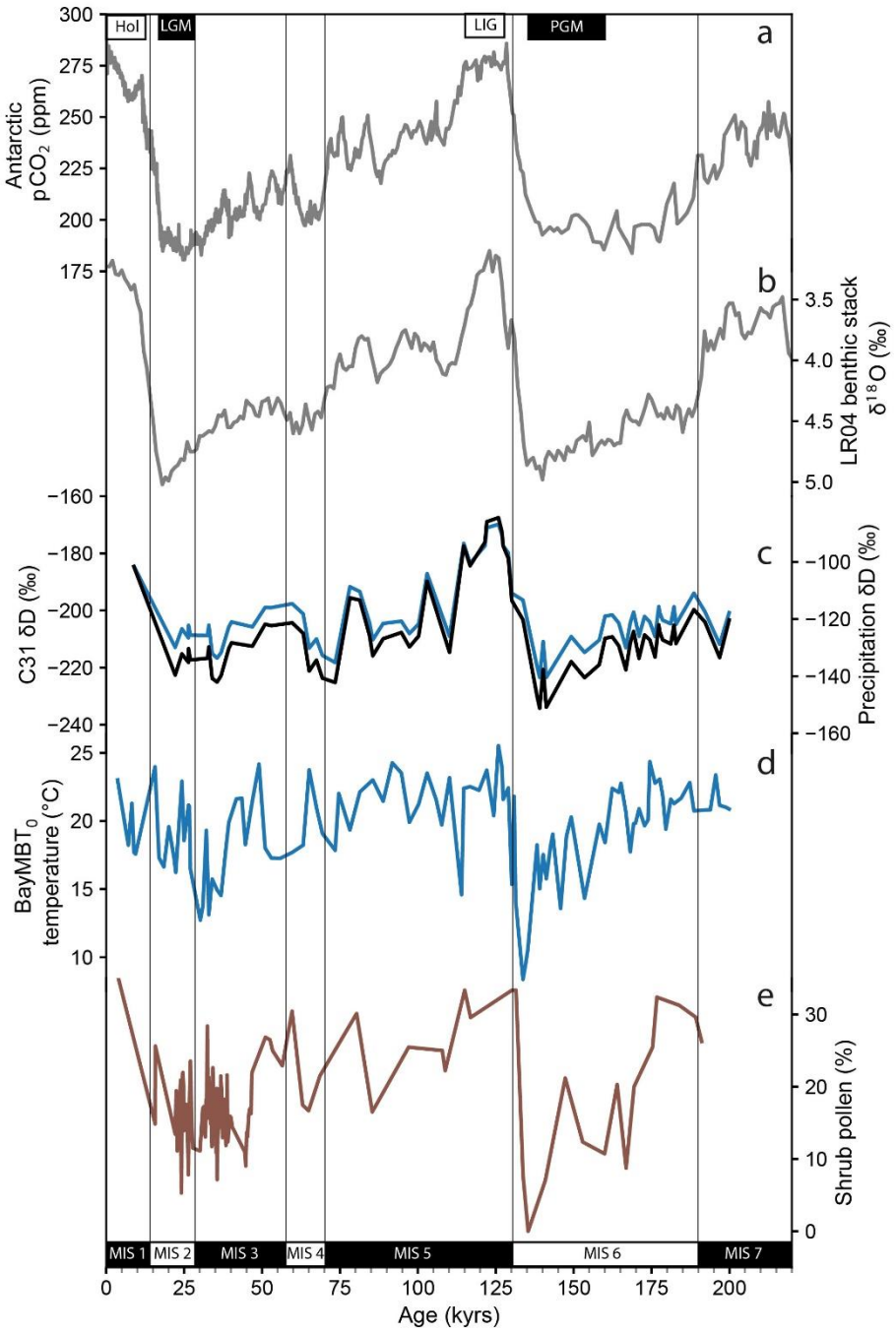

385

386 **Figure 4**. Comparison of Searles Lake plant wax δD_{31alk} and calculated δD_{precip} to global
387 climate data across two glacial interglacial cycles showing A) Antarctic pCO_2 record (Lüthi
388 et al., 2008), B) LR04 $\delta^{18}O$ benthic foraminifera stack (Lisiecki & Raymo, 2005), C) plant
389 wax C_{31} *n*-alkane δD (blue curve) and inferred precipitation δD after apparent fractionation
390 and ice volume correction (black curve). D) $BayMBT_0$ and E) shrub pollen%. Upper labels:
391 "Hol" = Holocene, "LGM" = Last glacial maximum, "LIG" = Last interglacial, "PGM" =
392 Penultimate glacial maximum. Lower labels: "MIS" = Marine isotope stage.

Comparison of the two glacial cycles in Searles Lake records suggests that the penultimate glacial maximum (PGM) was cooler and wetter compared to the last glacial maximum (LGM) which is in contrast to records of global climate change that show similar magnitudes of changes during both glacial maxima (Figure 4). The δD_{precip} is lower (Figure 4c), the $BayMBT_0$ temperature is 5° C lower (Figure 4d), and shrub pollen reaches a 200 ky minimum (Figure 4e) during the later stages of the penultimate glaciation compared to the LGM. The glacial-interglacial variations at Searles Lake are captured by changes in three independent, climate-sensitive proxies: plant wax, bacterial membrane lipids, and pollen microfossils. The climate changes that produce variations in these proxies are explored and evaluated further, in discussions of regional precipitation archives (Section 4.3), past water availability (Section 4.4), and past temperatures (Section 4.5).

3.3. Comparison with regional precipitation isotope archives

We compare the new 200 kyr Searles Lake plant wax reconstruction of δD_{precip} to regional speleothem $\delta^{18}O_{calcite}$ records (Figure 5). Devils Hole (located 120 km NE of Searles Valley) is a flooded cave with calcite deposition on the cave walls (Moseley et al., 2016). The Leviathan composite record (M. S. Lachniet, 2016), is comprised of stalagmite samples collected in Leviathan (270 km NE), Pinnacle (200 km E), and Lehman Caves (450 km NE), in Nevada (Figure 1a). All these caves are located in a similar precipitation isotope region, the Sierra Nevada rain shadow (Friedman et al., 2002), which justifies comparison with the plant wax record from Searles Lake. The cave records have been used extensively to determine the timing and amplitude of glacial-interglacial periods and their relationship to orbital cycles (Matthew S. Lachniet et al., 2014; Moseley et al., 2016; Winograd et al., 1992). Here we add an independent 200 kyr record from the plant wax precipitation isotope proxy

(Figure 5a).

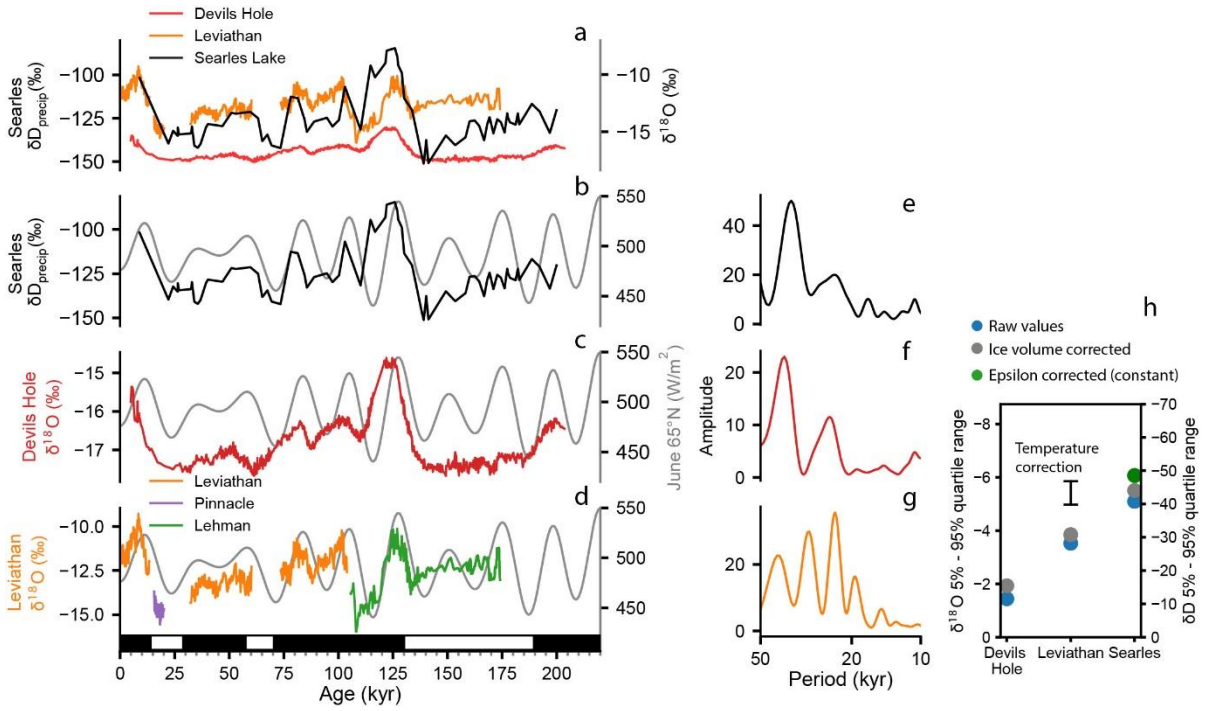

Figure 5. Comparison of plant wax and speleothem isotopic records. A) Searles Lake δD_{precip} (black, this study), Leviathan composite record $\delta^{18}O_{calcite}$ (orange; Lachniet et al., 2016) and Devils Hole $\delta^{18}O_{calcite}$ (red; Moseley et al., 2016) with the $\delta^{18}O$ axis scaled to account for the 8x greater mass dependent fractionation for hydrogen. B) Searles Lake δD_{precip} (black) and summer insolation at 65°N (gray). C) Devils Hole $\delta^{18}O_{calcite}$ and summer insolation at 65°N (gray). D) Leviathan composite record $\delta^{18}O_{calcite}$ (left) as in A but showing the individual caves, two of which (Lehman and Pinnacle), were adjusted for spatial gradients in precipitation isotopes (Lachniet et al., 2016). Black and white bars represent MIS stages. E – G) Weighted wavelet z transform frequency spectrum for the records in B, C, and D. H) 5 to 95 % quartile range for measured values (blue), and after corrections for ice volume (grey), cave temperature (Leviathan record, black bar) and plant wax $\varepsilon_{wax/w}$ (green). The $\delta^{18}O$ axis is scaled to account for the 8x difference in mass dependent fractionation between H and O. Ice volume-corrected Devils Hole shows the smallest range, whereas larger and comparable magnitudes are recorded at the temperature-corrected Leviathan composite record and Searles Lake.

The cave records and the plant wax precipitation isotope proxy all show similar glacial to interglacial pacing (Figure 5), with higher $\delta^{18}O$ and δD values during interglacial periods and lower values during glacials. Climate modelling studies have linked this isotopic signature to a southward displacement of the North Pacific low-level jet leading to increased cool season

precipitation (Oster et al., 2015; Tabor et al., 2021). The lower δD_{precip} values from plant waxes during the penultimate glaciation compared to the last glacial is not observed in the Devils Hole or Leviathan cave calcite records, perhaps because Searles Lake captured high altitude Sierra Nevada winter precipitation whereas the speleothems were recharged by lower altitude Great Basin precipitation more prone to changes in precipitation seasonality (Friedman et al., 1992). Both MIS 2 and 6 have similar insolation seasonality (Laskar et al., 2004) potentially explaining the similarity between the speleothem records. It should also be noted that the two glacial minima in the Leviathan composite record come from different caves hundreds of kilometres apart (Figure 5d). Spectral analyses of each record (Figure 5e–g) show that Searles Lake plant waxes and Devils Hole are paced predominantly by obliquity whereas the Leviathan composite record shows a precession signal.

For the obliquity pacing recorded in each archive, summer insolation maxima corresponds to higher $\delta^{18}O$ and δD, and the magnitude of change can be compared after accounting for the mass dependent fractionation scaling of 8 (Figure 5h). The amplitude of variability at Devils Hole, less than half that of Leviathan composite record, was attributed to aquifer averaging (M. Lachniet et al., 2017) and the slow rate of carbonate deposition (Moseley et al., 2016) relative to the stalagmite records from Leviathan composite record. In addition, cave temperature can modulate the amplitude of $\delta^{18}O_{calcite}$ through its control on equilibrium fractionation between water and calcite (Hendy, 1971; Kim & O'Neil, 1997). There is some evidence for this here as recent studies of triple oxygen isotopes have shown sensitivity to mineralization temperature at Leviathan and to evaporation at Lehman (Huth et al., 2022), although Devils Hole was not included in that study. A different study using clumped isotope methods suggested Devils Hole cave water remained within ±1°C over the past 600 kyrs because of the large aquifer size (Bajnai et al., 2021). We calculate a 6–10°C cooling

(consistent with our temperature reconstruction) during glacial maxima on the range in $\delta^{18}O_{calcite}$ in the Leviathan composite record (black bar Figure 5h).

Now we can add comparison to the plant wax δD record at Searles Lake, which shows a similar amplitude to the Leviathan composite record (Figure 5a, h). The correspondence of the glacial-interglacial changes and obliquity pacing with an independent proxy, such as plant wax in lake sediments, provides independent corroboration of the importance of obliquity pacing on large scale hydroclimate and atmospheric circulation. We note that obliquity and eccentricity are the dominant components of North American ice volume (Bintanja & Van De Wal, 2008) and as such changes in ice sheet extent may have been a forcing of hydroclimate with glacial-interglacial and obliquity signals recorded in both the Searles Lake and Devils Hole precipitation isotope archives. This means that the dominant precessional swings in the Leviathan composite $\delta^{18}O$ record may reflect cave air temperature changes which exert an effect on calcite fractionation. Plant wax δD_{precip} is not thought to be temperature sensitive, but it carries uncertainty associated with fractionation, aridity, and plant type. The similarity between the plant wax and cave records supports the obliquity pacing of precipitation isotopes, but their climate significance is less clear. Although precipitation isotopes are valued hydrological tracers that capture the obliquity pacing and glacial-interglacial climate, they remain an indirect proxy for moisture availability on the landscape, leaving a need for additional proxy constraints on hydroclimate.

3.4. Searles Lake salinity and regional moisture availability

3.4.1. Salinity proxies

Searles Lake biomarkers contain a record of salinity, which inversely covaries with lake depth in terminal lakes (Olson & Lowenstein, 2021). We compare results from two indices

responsive to lake salinity, the ACE index (Figure 6a) previously reported in Peaple et al. (2021), and the IR_{6+7me} (Figure 6b) newly measured here for comparison and to differentiate the times of freshwater conditions. While the ACE index (Turich and Freeman, 2011), is sensitive to lake hypersalinity (H. Wang et al., 2013), it loses sensitivity below 60 psu (He et al., 2020). Below 100 psu the IR_{6+7me} index has promise, although it performs worse than ACE above that threshold (He et al., 2020). We test both approaches and find that there is a moderate positive correlation between ACE and IR_{6+7me} in the bottom section of the core (76-50 m, $r = 0.43$, $p > 0.01$) within carbonate muds of a perennial, predominantly saline lake. No correlation exists in the interbedded muds and salts deposited in perennial saline to hypersaline lakes (50–6 m, $r = 0$, $p = 0.6$), above the salinity limit of IR_{6+7me} (Sup Figure S6). ACE values range from 0 to 100 and IR_{6+7me} range from 0.4 to 0.8. Low ACE values were found in thick muds (25–22 m and 29–28 m) deposited during deeper lake phases. High ACE was measured in interbedded muds and salts (36–34 m depth) deposited in perennial hypersaline lakes that precipitated evaporite salts including trona and burkeite (Olson and Lowenstein, 2021; Olson et al., in review). IR_{6+7me} (0.60) is lower (i.e. fresher) in hypersaline lake stages than in deeper lake mud units (0.66) suggesting that IR_{6+7me} fails to register the salty conditions.

However, the lowest IR_{6+7me} indicates a fresh water lake at 140–130 ka where we also observe unique BIT and %GDGT-0 values (0.3 and 0.6 respectively) that reflect the highest lake level and freshest water of the 200 kyr record. ACE is low between 140-130 ka, but there are several other periods with similarly low ACE in the Searles Lake record (Figure 6a). Both salinity proxies show precessional pacing, in contrast to the obliquity-dominated δD_{precip} (Figure S5c). Cross spectral analysis shows both salinity proxies have phase coherence in the precessional and obliquity bands (1/19–1/45 kyrs) between 175–90 kyrs (Figure S5b). Strong

precessional variability is also present in the % total organic matter measured in Baldwin Lake (Southern California) sediments, between 125–75 kyrs (Glover et al., 2017), suggesting that changes in summer insolation were important in controlling regional lake paleoenvironmental conditions during MIS6–MIS5. Higher frequency coherence exists between 1/10–1/17 kyrs bands than between 90–50 kyrs and then weaker antiphase coherence between 50–12 kyrs is associated with proxy discrepancy across changing salinities described. BIT and %GDGT-0 (Figure 6c) remain close to 1 and >1 respectively throughout much of the 200 kyr record, indicating a stratified lake with a shallow oxycline (Baxter et al., 2021).

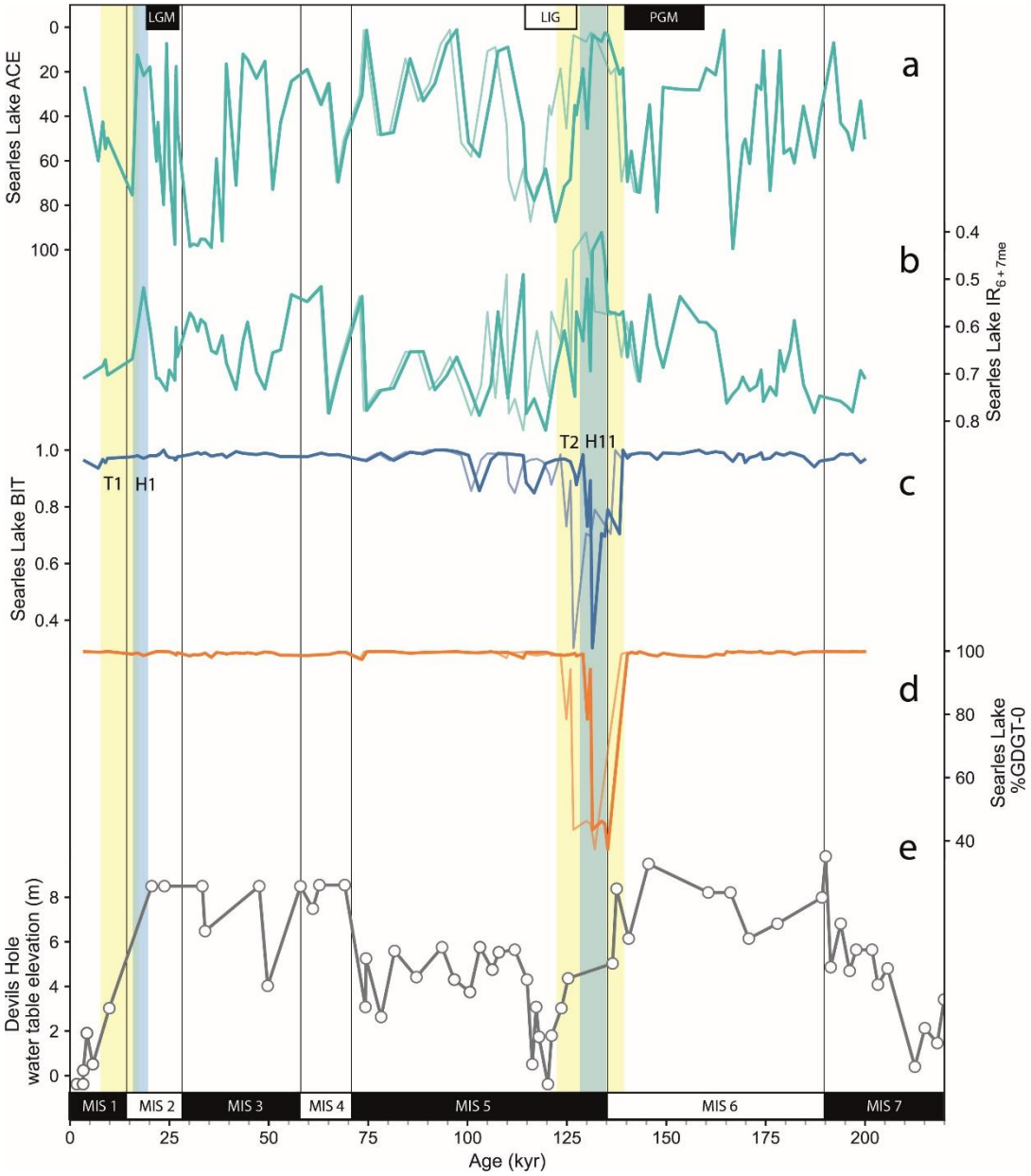

519

520 **Figure 6**. Biomarker evidence that the late MIS 6 pluvial was a fresher water lake than the
521 late MIS 2 pluvial. Water balance reconstructions Searles Lake: A) ACE, B) IR_{6+7me}, C) BIT
522 D) %GDGT-0, and E) Devils Hole water table elevation (Wendt et al., 2018). Age model
523 without tie point is plotted for all GDGT indices as a thin faint line. Terminations 1 and 2 are
524 highlighted with yellow shading and Heinrich 1 and 11 are highlighted with blue shading.
525 Upper labels: "LGM" = Last glacial maximum, "LIG" = Last interglacial, "PGM" =
526 Penultimate glacial maximum. Lower labels: "MIS" = Marine isotope stage.

527

528 **3.4.2. Comparison to regional moisture availability records**

529 We compare biomarker records of salinity based on ACE, IR_{6+7me} as well as BIT and

530 %GDGT-0 evidence for limnological conditions in Searles Lake, to the nearby Devils Hole

record of water table elevation from calcite deposits (Wendt et al., 2018). The Searles Lake ACE (Figure 6a) and IR_{6+7me} (Figure 6b) records share key similarities with the Devils Hole water table (Figure 6d) including: a more saline lake corresponds with low water table elevations during the previous interglacial (Eemian), and fresher conditions accompany relatively high water tables during Heinrich 1 and Heinrich 11.

In both archives we find MIS 6 was wetter than MIS 2. The mean ACE and IR_{6+7me} were 10 lower and 0.1 higher respectively during MIS 6 relative to MIS 2 Searles Lake. Evidence for wetter conditions during MIS 6 at Devils Hole comes from subaqueous calcite (Wendt et al., 2018), which formed when the water table was at a higher elevation than 9.5 m (maximum height of calcite collected by Wendt et al., 2018) and are much thicker in MIS 6 compared to MIS 2, suggesting longer and more frequent water table highstands.

3.4.3. Lake outflow

Previous studies have identified 7 periods of outflow from Searles Lake into Panamint Valley during glacial pluvials during the last 2 Ma (Jannik et al., 1991; Smith et al., 1983). Searles Lake shoreline deposits indicate brief episodes of outflow occurred between 15–12 kyr (Lin et al., 1998; Smith, 2009) which resulted in an 180–200 m deep lake being present in Panamint Valley during periods of MIS 2 (Jayko et al., 2008). During MIS 6, Searles Lake shoreline deposits (Smith, 2009) and chlorine transfer budget (Jannik et al., 1991) suggests a period of intensive overflow into Panamint Valley which resulted in the formation of a >300m deep Lake Panamint which overspilled into Death Valley (Jayko et al., 2008). This overspill resulted in Lake Manly being deeper during MIS 6 than MIS2, likely as a direct result of inflow from Lake Panamint (Forester et al., 2005; Roberts & Spencer, 1998). Further upstream, dates of lake highstands and outflows suggest that Mono Lake was possibly

554 overspilling into the Owens River catchment during MIS 6 but not during MIS 2 (Reheis et
555 al., 2002; Reheis pers. comm., 1/20/2022).

556 We find evidence suggesting unique limnological conditions existed at Searles Lake between
557 140–130 ka during late MIS 6. In comparison to high BIT and %GDGT-0 indexes (~1 and
558 >99% respectively) in most of the 200 kyr record, indicating stratified low productivity lakes,
559 both indices decrease to medians of 0.72 and 46% respectively, between 140–130 ka (Figure
560 6c), and IR_{6+7Me} values reach a freshwater minimum. Modern studies of Lake Challa suggest
561 that crenarchaeol-producing Thaumarchaeota live above a shallow oxycline, and
562 methanogenic archaea, which produce GDGT-0, occur below the oxycline of an anoxic lake
563 (Baxter et al., 2021). Searles Lake sediments typically have low crenarchaeol relative to
564 brGDGTs (high BIT) and GDGT-0 (high %GDGT-0), suggesting salinity stratified and/or
565 low oxygen conditions. But biomarkers from 140–130 ka denote freshwater, high lake
566 productivity and a vigorously mixed water column with deep oxygenation. Lake overturning
567 is enabled in freshwater systems where winter cooling causes surface waters to sink, also
568 assisted by the turbulence of water inflow and outflow (Rimmer et al., 2011). While much of
569 SLAPP-SLRS17 consists of laminated aragonite thought to reflect salinity-stratified
570 conditions, this portion of the core is characterized by massive mud deposits (Figure S5).
571 These massive mud deposits likely reflect well-mixed lake conditions that allowed for
572 bioturbation.

573 While Searles was likely overflowing during MIS 2, we do not see a decrease in BIT or
574 %GDGT-0, suggesting that the lake was not well oxygenated and/or fresh. This could suggest
575 that Searles was not vigorously outflowing for any extended period of time during MIS 2.
576 Additionally, constant sediment deposition on the lake floor from MIS 6 to the present has

resulted in the lake floor becoming shallower with time, impacting the lake depth necessary to reach the sill elevation. During MIS 6 the lake depth required for spill over was 274m, but during MIS 2 this reduced to 225m (Smith, 2009). Given that Searles Lake was vigorously outflowing during late MIS 6 under 45m deeper water levels than MIS 2, we can infer that inflow into Searles must have been greater during MIS 6 than MIS 2.

3.4.4. Heinrich Stadials 1 and 11

Benthic $\delta^{18}O$ values (Lisiecki & Raymo, 2005) and atmospheric pCO_2 (Lüthi et al., 2008) are broadly similar in amplitude during the last two glacial cycles (Figure 4a, b). However the PGM has a longer duration than the LGM (Jouzel et al., 1993) which is manifested regionally by the extended high water table at Devils Hole (Wendt et al., 2018). At Searles Lake, the freshest and highest lake levels are reconstructed not during the PGM but during H11. Terminations 1 and 2 differ in terms of their sea level rise, T2 being a continuous, rapid rise, whereas T1 has a two-step rise (Clark et al., 2020). T2 has a stronger insolation forcing in terms of Northern Hemisphere summer solstice maximum (Bova et al., 2021). We note the difference in terms of the wet climate state captured in the Searles Lake setting: we find peak wetness at T2 not T1. While Sierra Nevada glacial melt could be a transient contributor, extended wet conditions point to increased precipitation. Tracers of cave infiltration including trace element ratios, Sr/Ca, $^{87}Sr/^{86}Sr$ and carbon isotopic evidence from Lehman cave, Nevada, also suggest that H11 was wetter than the preceding MIS6 glacial maximum and terminated rapidly within 2 kyrs. A disconnect between P–E and $\delta^{18}O_{calcite}$ was identified from Lehman cave (Cross et al., 2015), which matches the lack of covariance we observe between the Searles Lake δD_{precip} and our ACE and IR_{6+7me} proxies, suggesting that this is a regional climatic feature and not constrained by one cave. This disconnect could be related to

either increasing temperatures and/or changing seasonality/source of precipitation (Cross et al., 2015). Model simulations link north Atlantic cooling during Heinrich stadials to pluvials in southwestern North America (D. McGee et al., 2018). Freshwater inputs to the North Atlantic slow the Atlantic Meridional Overturning Circulation, leading to winter cooling in the Northern Hemisphere, causing the Inter Tropical Convergence Zone to shift southward as also seen in the proxy record (Allison W Jacobel et al., 2016). These changes intensify the northern Hadley Cell, accelerating the subtropical jet and increasing the winter season delivery of atmospheric river precipitation to the southwestern North America (D. McGee et al., 2018). Precipitation from tropical/sub-tropical atmospheric rivers is relatively enriched in the heavier isotopes of D and ^{18}O, compared to North Pacific derived moisture (Berkelhammer et al., 2012). Thus, the increase in δD_{precip} we observe at Searles Lake during H11 and the increase in $\delta^{18}O_{calcite}$ seen in Lehman Cave (Cross et al., 2015) is consistent with this hypothesis. Central Pacific ITCZ southward migration appears to be substantially greater in T2 than in T1 (A. W. Jacobel et al., 2017), consistent with the deeper lake we detect at Searles. Temperature changes likely play a secondary role in amplifying the δD_{precip} signal (Dansgaard, 1964).

The biomarker evidence shows that the pluvial associated with Heinrich 11 produced deeper, fresher lakes than H1. Coastal pollen records form central California marine core ODP Site 1018 corroborate this pluvial comparison, finding a 20% greater decrease in shrub pollen associated with the T2 extreme wet event compared to the T1 pluvial. The T2 pluvial is wetter than all other glacial terminations of the past 600 kyrs as recorded by ODP Site 1018 pollen and by the Searles to Panamint chlorine transfer budget (Jannik et al., 1991).

3.4.5. Timing of the T2 pluvial

Regarding the timing of the pluvial close to H11, we wish to note the implications of the age model selection represented with the comparison on Figure 6. The SLAPP-SRLS17 preferred age model based on U/Th incorporates an age tie point between the Leviathan composite $\delta^{18}O_{calcite}$ and Searles Lake δD of C_{31} alkane, with an age of 126.5 kyr, at a gap in the U/Th constraints (Section 1.2). This age model places the peak of the vigorous overflow event in Searles Valley (Figure 6a, b, c, d and e) is at 131.4 kyr making it coincident with H11 (Cross et al., 2015). Without the tie point the U/Th-only age model places the overflow event later at 126.6 kyr. Regional climate records from southwestern North America uniformly suggest that MIS5e was relatively dry (e.g. Litwin et al., 1999; Woolfenden, 2003; Cross et al., 2015; Wendt et al., 2018). Based on the assumption that the tie point to regional cave records is appropriate, the microbial lipid record from the Searles Basin supports wet conditions during H11 followed by a shift to drier conditions at the beginning of MIS5.

3.5. Terrestrial temperatures

We are able to contribute to sparse evidence for terrestrial temperature change on land with the new biomarker records from Searles Lake (Figure 7). We reconstruct mean annual temperature of months above freezing (Figure 7a) of Searles Lake using the $BayMBT_0$ calibration of the bacterial lipid MBT'_{5Me} index in global lakes (Martínez-Sosa et al., 2021). This record overlaps with the 33–9 kyr record from Lake Elsinore with the same proxy (Feakins et al., 2019), recalibrated with the same MAF calibration here (Figure 7a). Both lakes show 10˚C glacial-to-Holocene warming and similar magnitude variability within glacials, with notably warm intervals during the glacial from 50–30 kyrs at Searles (22°C) corroborating reports of warm times during the last glacial in the region (Feakins et al.,

2019). While brGDGT reconstructions can suffer from biases induced by shallow lake depth, hypersalinity (He et al., 2020) and high alkalinity (Martínez-Sosa et al., 2021) in part related to more influence from allochthonous inputs from soil derived brGDGTs in less productive, saline lakes (Martínez-Sosa et al., 2021), our tests corroborate use of the $BayMBT_0$ lake calibration (see Supplemental Information). We note reconstructed temperatures from both Searles Lake and Lake Elsinore during the Holocene are similar to modern measured MAF. Independent corroboration of the magnitude of the terrestrial deglacial warming comes from noble gas groundwater paleotemperature reconstructions from the Mojave Desert (Kulongoski et al., 2009) and San Diego (Seltzer et al., 2021) that capture evidence for 7–10°C deglacial warming (Figure 7b).

In the 200 kyr $BayMBT_0$ record from Searles Lake we identify the penultimate glacial as colder than the last glacial. That cooling occurred between 215–150 kyr, followed by a sharp warming during T2 (140–130 kyr) and relative temperature stability between 130–50 kyr, pronounced cooling from 50–18 kyr and then deglacial warming, previously described. Within the low BIT interlude (BIT = 0.3) of the penultimate glaciation at 131.4 kyr, we were able to obtain a single archaeal, isoGDGT-based TEX_{86} estimate of lake surface temperature applying the lake calibration (Tierney et al., 2010) to one sample yielding an estimate of 12 ± 2°C (Figure 7a). This sample also yielded a $BayMBT_0$ temperature estimate of 14 ± 3°C, equivalent within calibration uncertainties. We note that the coldest temperatures are also associated with the freshest conditions in the lake (low ACE, lowest IR_{6+7me}) and the indication of overflow into Panamint based on the %GDGT-0 and BIT. Overturning in lakes increases brGDGT production and export to sediments (Loomis et al., 2014), which could result in a larger proportion of lake derived bGDGT compared to allochthonous inputs. Given that soil calibration of MBT'_{5Me} underestimates temperatures when applied to lakes

(Martínez-Sosa et al., 2021), a decreased input of soil-derived brGDGTs could lead to a decrease in reconstructed temperatures independent of a change in air temperature.

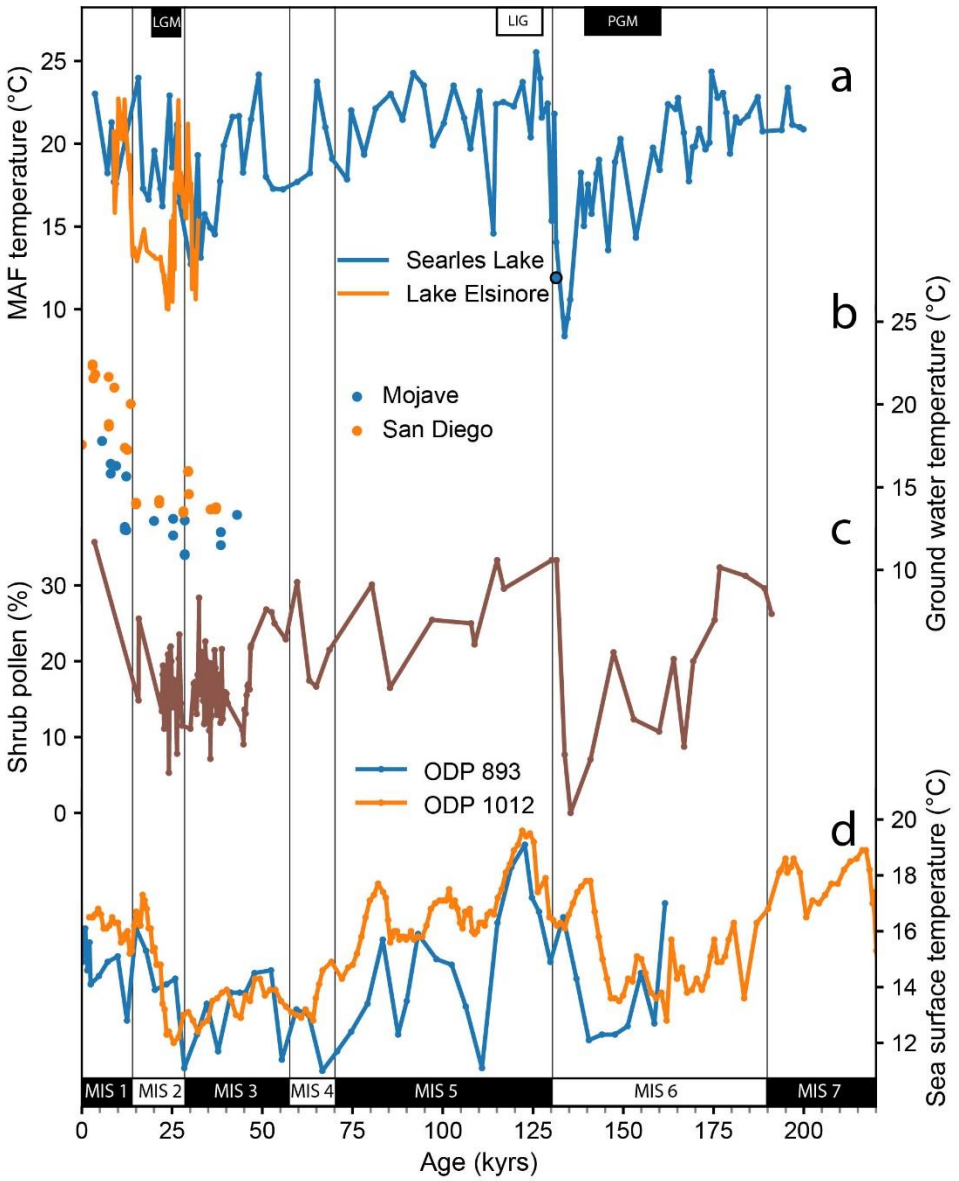

Figure 7. Local and regional temperature records over the past 200 kyr. A. Searles Lake (blue line; this study) and Lake Elsinore (orange line; Feakins et al., 2019) recalibrated to MAF using Martinez Sosa et al., (2021) brGDGT temperature records, using the lake MBT'_{5Me} $BayMBT_0$ calibration to mean temperature from months above freezing (MAF). TEX_{86} calibrated to lake surface temperature (black dot) (Tierney et al., 2010). B) Noble gas derived ground water temperature records (Mojve: Kulongoski et al., 2009; San Diego: Seltzer et al., 2021). Comparison temperature responsive vegetation change showing C) shrub pollen % (Amaranthaceae and Asteraceae; this study). D) Alkenone based sea surface temperature (SST) records (ODP 1012, ODP 893: Herbert et al., 2001, 1995).

Glacial-interglacial pacing dominates the SSTs (Figure 7c), which have a smaller amplitude (5°C) compared to the terrestrial records, that vary by 10°C between 50–30 ka (Figure 7a). Terrestrial changes in vegetation covary with air temperature, for example warm interludes around 50 ka (Figure 7a) correspond to increased pollen from desert shrub taxa (Figure 7c), confirming that hot conditions matter to regional moisture availability. This indicates the importance of terrestrial temperature reconstructions to understand the relationships between hydroclimate and vegetation on land.

4. Conclusions

We present a new biomarker and pollen record from the SLAPP core drilled in Searles Lake spanning the past 200 kyr. We show evidence from pollen and plant wax for vegetation change and find that shrub pollen responds to glacial-interglacial temperature change. We show that the plant wax *n*-alkane-based proxy for δD_{precip} is characterised by large glacial to interglacial and obliquity changes, likely driven by variations in ice volume. There is a strong correlation ($r = 0.75$, $p > 0.01$) determined by non-parametric methods that account for serial correlation (Ebisuzaki, 1997) between changes in δD_{precip} and changes in $\delta^{18}O_{calcite}$ from the nearby Devils Hole speleothem. The similar pacing suggests that both archives are recording precipitation isotopic composition, however the Searles Lake δD_{precip} record shows larger amplitude changes.

We also present more direct indicators of moisture availability. The ACE index of lake salinity as well as IR_{6+7me} are consistent with lake core lithology and shoreline markers. We find similarities between Devils Hole water table and regional lake depths, with pluvials during glacials and drier interglacial conditions. However we find that Searles Lake was likely deeper during the penultimate glacial, MIS 6, compared to MIS 2, with the wettest

conditions occurring during Termination 2, especially Heinrich stadial 11. During H11, Searles Lake was well-mixed and overflowed into Panamint Basin, interpreted from the large decrease in BIT and %GDGT-0. In comparison, Searles Lake remained a stratified, saline, terminal lake during the last lake highstand in Heinrich 1.

Both brGDGT-derived temperatures and the proportion of shrub pollen increase during interglacial periods, although glacial temperature minima differ with terminal MIS 6 being 4°C cooler than MIS 2. We find less shrub pollen, a fresher lake and more D-depleted precipitation in the T2 pluvial, providing confidence that the T2 pluvial was wetter than the T1 pluvial from these independent lines of evidence from the sediments in the Searles Lake core. This 200 kyr record reveals differences between the two glacial pluvials and between two interglacials, highlighting the sensitivity of southwestern North America's hydroclimate.

Acknowledgements

The plant wax study and GRA (Peaple) were supported by U.S. National Science Foundation Grant NSF-EAR-1903665 to S.F., GDGT analyses were supported by the Packard Fellowship for Science and Engineering to J.T., and the pollen analyses were supported by a sub-award to T.B. from NSF-EAR-1903659 to T.L. Drilling was supported by the Comer Science and Education Foundation Grant to D.M. and T.L. We thank Searles Valley Minerals for access and Jade Zimmermann in particular. Sample material used in this project was provided by LacCore. We thank the SLAPP team involved in coring and collaborative discussions of surroundings and paleoenvironment, as well as Marith Reheis for discussion of Lake Russell overflow, Jay Quade for plant identification in the Mojave Desert, Alan Juarez for field assistance in the San Bernardino Mountains and Patrick Murphy for assistance measuring GDGTs.

Author contributions**:** SF, DM and TL designed the study and acquired the funding; MP conducted the biomarker analyses, graphed the data and wrote the paper; SF supervised MP and contributed to writing; TB conducted pollen analyses and contributed to writing; JT

supported GDGT analyses; KO contributed sediment stratigraphy; JS contributed the age model; all authors contributed.

Conflict of Interest

The authors declare no financial conflicts of interests for any author or their affiliations.

Data Availability Statement

Data files are archived at the NOAA paleoclimatology database at https://www.ncdc.noaa.gov/paleo/study/xxxxx (Peaple et al., 2022).

Supporting Information

Supporting information may be found in the online version of this article.

References

Bacon, S. N., Jayko, A. S., Owen, L. A., Lindvall, S. C., Rhodes, E. J., Schumer, R. A., & Decker, D. L. (2020). A 50,000-year record of lake-level variations and overflow from Owens Lake, eastern California, USA. *Quaternary Science Reviews*, *238*, 106312. https://doi.org/10.1016/j.quascirev.2020.106312

Bajnai, D., Coplen, T. B., Methner, K., Löffler, N., Krsnik, E., & Fiebig, J. (2021). Devils Hole Calcite Was Precipitated at ±1°C Stable Aquifer Temperatures During the Last Half Million Years. *Geophysical Research Letters*, *48*(11). https://doi.org/10.1029/2021GL093257

Baxter, A. J., van Bree, L. G. J., Peterse, F., Hopmans, E. C., Villanueva, L., Verschuren, D., & Sinninghe Damsté, J. S. (2021). Seasonal and multi-annual variation in the abundance of isoprenoid GDGT membrane lipids and their producers in the water column of a meromictic equatorial crater lake (Lake Chala, East Africa). *Quaternary Science Reviews*, *273*, 107263. https://doi.org/10.1016/J.QUASCIREV.2021.107263

Berkelhammer, M., Stott, L., Yoshimura, K., Johnson, K., & Sinha, A. (2012). Synoptic and mesoscale controls on the isotopic composition of precipitation in the western United States. *Climate Dynamics*, *38*(3–4), 433–454. https://doi.org/10.1007/s00382-011-1262-3

Bhattacharya, T., Tierney, J. E., Addison, J. A., & Murray, J. W. (2018). Ice-sheet modulation of deglacial North American monsoon intensification. *Nature Geoscience*, 1. https://doi.org/10.1038/s41561-018-0220-7

Bintanja, R., & Van De Wal, R. S. W. (2008). North American ice-sheet dynamics and the onset of 100,000-year glacial cycles. *Nature 2008 454:7206*, *454*(7206), 869–872. https://doi.org/10.1038/nature07158

765 Bischoff, J. L., & Cummins, K. (2001). Wisconsin Glaciation of the Sierra Nevada (79,000-
766 15,000 yr B.P.) as recorded by rock flour in sediments of Owens Lake, California.
767 *Quaternary Research*, *55*(1), 14–24. https://doi.org/10.1006/qres.2000.2183
768 Bova, S., Rosenthal, Y., Liu, Z., Godad, S. P., & Yan, M. (2021). Seasonal origin of the
769 thermal maxima at the Holocene and the last interglacial. *Nature 2021 589:7843*,
770 *589*(7843), 548–553. https://doi.org/10.1038/s41586-020-03155-x
771 Byrne, R. (1982). Preliminary pollen analysis of Deep Sea Drilling Project Leg 64 Hole 480
772 (Cores 1-11).
773 Campbell, I. D., McDonald, K., Flannigan, M. D., & Kringayark, J. (1999). Long-distance
774 transport of pollen into the Arctic. *Nature*, *398*(6731), 29–30.
775 https://doi.org/10.1038/19891
776 Clark, P. U., He, F., Golledge, N. R., Mitrovica, J. X., Dutton, A., Hoffman, J. S., & Dendy,
777 S. (2020). Oceanic forcing of penultimate deglacial and last interglacial sea-level rise.
778 *Nature 2020 577:7792*, *577*(7792), 660–664. https://doi.org/10.1038/s41586-020-1931-
779 7
780 Cross, M., McGee, D., Broecker, W. S., Quade, J., Shakun, J. D., Cheng, H., et al. (2015).
781 Great Basin hydrology, paleoclimate, and connections with the North Atlantic: A
782 speleothem stable isotope and trace element record from Lehman Caves, NV.
783 *Quaternary Science Reviews*, *127*, 186–198.
784 https://doi.org/10.1016/J.QUASCIREV.2015.06.016
785 Dansgaard, W. (1964). Stable isotopes in precipitation. *Tellus*, *16*(4), 436–468.
786 https://doi.org/10.1111/j.2153-3490.1964.tb00181.x
787 Davis, O. K. (1998). Palynological evidence for vegetation cycles in a 1.5 million year pollen
788 record from the Great Salt Lake, Utah, USA. *Palaeogeography, Palaeoclimatology,*
789 *Palaeoecology*, *138*(1–4), 175–185. https://doi.org/10.1016/S0031-0182(97)00105-3
790 Diefendorf, A. F., Leslie, A. B., & Wing, S. L. (2015). Leaf wax composition and carbon
791 isotopes vary among major conifer groups. *Geochimica et Cosmochimica Acta*, *170*,
792 145–156. https://doi.org/10.1016/j.gca.2015.08.018
793 Ebisuzaki, W. (1997). A method to estimate the statistical significance of a correlation when
794 the data are serially correlated. *Journal of Climate*, *10*(9), 2147–2153.
795 https://doi.org/10.1175/1520-0442(1997)010<2147:AMTETS>2.0.CO;2
796 Faith, D. P., Minchin, P. R., & Belbin, L. (1987). Compositional dissimilarity as a robust
797 measure of ecological distance. *Vegetatio 1987 69:1*, *69*(1), 57–68.
798 https://doi.org/10.1007/BF00038687
799 Fasham, M. J. R. (1977). A Comparison of Nonmetric Multidimensional Scaling, Principal
800 Components and Reciprocal Averaging for the Ordination of Simulated Coenoclines,
801 and Coenoplanes. *Ecology*, *58*(3), 551–561. https://doi.org/10.2307/1939004
802 Feakins, S. J., Wu, M. S., Ponton, C., Galy, V., & West, A. J. (2018). Dual isotope evidence
803 for sedimentary integration of plant wax biomarkers across an Andes-Amazon elevation
804 transect. *Geochimica et Cosmochimica Acta*, *242*, 64–81.
805 https://doi.org/10.1016/j.gca.2018.09.007
806 Feakins, S. J., Wu, M. S., Ponton, C., & Tierney, J. E. (2019). Biomarkers reveal abrupt
807 switches in hydroclimate during the last glacial in southern California. *Earth and*
808 *Planetary Science Letters*, *515*, 164–172. https://doi.org/10.1016/j.epsl.2019.03.024
809 Forester, R. M., Lowenstein, T. K., & Spencer, R. J. (2005). An ostracode based
810 paleolimnologic and paleohydrologic history of Death Valley: 200 to 0 ka. *GSA Bulletin*,

117(11–12), 1379–1386. https://doi.org/10.1130/B25637.1

Freimuth, E. J., Diefendorf, A. F., Lowell, T. V., & Wiles, G. C. (2019). Sedimentary n-alkanes and n-alkanoic acids in a temperate bog are biased toward woody plants. *Organic Geochemistry*, *128*, 94–107. https://doi.org/10.1016/j.orggeochem.2019.01.006

Friedman, I., Smith, G. I., Gleason, J. D., Warden, A., & Harris, J. M. (1992). Stable isotope composition of waters in southeastern California 1. Modern precipitation. *Journal of Geophysical Research*, *97*(D5), 5795. https://doi.org/10.1029/92JD00184

Friedman, I., Harris, J. M., Smith, G. I., & Johnson, C. A. (2002). Stable isotope composition of waters in the Great Basin, United States 1. Air-mass trajectories. *Journal of Geophysical Research: Atmospheres*, *107*(D19), ACL 14-1. https://doi.org/10.1029/2001JD000565

Glover, K. C., MacDonald, G. M., Kirby, M. E., Rhodes, E. J., Stevens, L., Silveira, E., et al. (2017). Evidence for orbital and North Atlantic climate forcing in alpine Southern California between 125 and 10 ka from multi-proxy analyses of Baldwin Lake. *Quaternary Science Reviews*, *167*, 47–62. https://doi.org/10.1016/J.QUASCIREV.2017.04.028

He, Y., Wang, H., Meng, B., Liu, H., Zhou, A., Song, M., et al. (2020). Appraisal of alkenone- and archaeal ether-based salinity indicators in mid-latitude Asian lakes. *Earth and Planetary Science Letters*, *538*, 116236.

Hendy, C. H. (1971). The isotopic geochemistry of speleothems—I. The calculation of the effects of different modes of formation on the isotopic composition of speleothems and their applicability as palaeoclimatic indicators. *Geochimica et Cosmochimica Acta*, *35*(8), 801–824. https://doi.org/10.1016/0016-7037(71)90127-X

Herbert, T. D., Yasuda, M., & Burnett, C. (1995). Glacial-Interglacial Sea-Surface Temperature Record Inferred from Alkenone Unsaturation indices, Site 893, Santa Barbara Basin. In *Proceedings of the Ocean Drilling Program, 146 Part 2 Scientific Results* (Vol. 146). https://doi.org/10.2973/odp.proc.sr.146-2.301.1995

Herbert, T. D., Schuffert, J. D., Andreasen, D., Heusser, L., Lyle, M., Mix, A., et al. (2001). Collapse of the California current during glacial maxima linked to climate change on land. *Science*, *293*(5527), 71–76. https://doi.org/10.1126/SCIENCE.1059209

Heusser, L. E., Kirby, M. E., & Nichols, J. E. (2015). Pollen-based evidence of extreme drought during the last Glacial (32.6-9.0 ka) in coastal southern California. *Quaternary Science Reviews*, *126*, 242–253. https://doi.org/10.1016/j.quascirev.2015.08.029

Holmgren, C. A., Betancourt, J. L., & Rylander, K. A. (2010). A long-term vegetation history of the Mojave-Colorado desert ecotone at Joshua Tree National Park. *Journal of Quaternary Science*, *25*(2), 222–236. https://doi.org/10.1002/jqs.1313

Hopmans, E. C., Schouten, S., & Sinninghe Damsté, J. S. (2016). The effect of improved chromatography on GDGT-based palaeoproxies. *Organic Geochemistry*, *93*, 1–6. https://doi.org/10.1016/j.orggeochem.2015.12.006

Huth, T. E., Passey, B. H., Cole, J. E., Lachniet, M. S., McGee, D., Denniston, R. F., et al. (2022). A framework for triple oxygen isotopes in speleothem paleoclimatology. *Geochimica et Cosmochimica Acta*, *319*, 191–219. https://doi.org/10.1016/J.GCA.2021.11.002

Jacobel, A. W., McManus, J. F., Anderson, R. F., & Winckler, G. (2017). Climate-related response of dust flux to the central equatorial Pacific over the past 150 kyr. *Earth and Planetary Science Letters*, *457*, 160–172. https://doi.org/10.1016/J.EPSL.2016.09.042

857 Jacobel, Allison W, McManus, J. F., Anderson, R. F., & Winckler, G. (2016). Large deglacial
858 shifts of the Pacific intertropical convergence zone. *Nature Communications*, *7*(1), 1–7.
859 Jannik, N. O., Phillips, F. M., Smith, G. I., & Elmore, D. (1991). A 36Cl chronology of
860 lacustrine sedimentation in the Pleistocene Owens River system. *Geological Society of*
861 *America Bulletin*, *103*(9), 1146–1159.
862 Jasechko, S., Lechler, A., Pausata, F. S. R., Fawcett, P. J., Gleeson, T., Cendon, D. I., et al.
863 (2015). Late-glacial to late-Holocene shifts in global precipitation δ18O. *Climate of the*
864 *Past*, *11*(10), 1375–1393. https://doi.org/10.5194/CP-11-1375-2015
865 Jayko, A. S., Forester, R. M., Kaufman, D. S., Phillips, F. M., Yount, J. C., McGeehin, J., &
866 Mahan, S. A. (2008). Late Pleistocene lakes and wetlands, Panamint Valley, Inyo
867 County, California. In *Special Paper of the Geological Society of America* (Vol. 439, pp.
868 151–184). https://doi.org/10.1130/2008.2439(07)
869 De Jonge, C., Hopmans, E. C., Zell, C. I., Kim, J. H., Schouten, S., & Sinninghe Damsté, J.
870 S. (2014). Occurrence and abundance of 6-methyl branched glycerol dialkyl glycerol
871 tetraethers in soils: Implications for palaeoclimate reconstruction. *Geochimica et*
872 *Cosmochimica Acta*, *141*, 97–112. https://doi.org/10.1016/j.gca.2014.06.013
873 Jouzel, J., Barkov, N. I., Barnola, J. M., Bender, M., Chappellaz, J., Genthon, C., et al.
874 (1993). Extending the Vostok ice-core record of palaeoclimate to the penultimate glacial
875 period. *Nature 1993 364:6436*, *364*(6436), 407–412. https://doi.org/10.1038/364407a0
876 Kim, S. T., & O'Neil, J. R. (1997). Equilibrium and nonequilibrium oxygen isotope effects in
877 synthetic carbonates. *Geochimica et Cosmochimica Acta*, *61*(16), 3461–3475.
878 https://doi.org/10.1016/S0016-7037(97)00169-5
879 Koehler, P. A., Anderson, R. S., & Spaulding, W. G. (2005). Development of vegetation in
880 the Central Mojave Desert of California during the late Quaternary. *Palaeogeography,*
881 *Palaeoclimatology, Palaeoecology*, *215*(3–4), 297–311. Retrieved from
882 https://www.researchgate.net/publication/222663179_Development_of_vegetation_in_t
883 he_Central_Mojave_Desert_of_California_during_the_late_Quaternary
884 Kulongoski, J. T., Hilton, D. R., Izbicki, J. A., & Belitz, K. (2009). Evidence for prolonged
885 El Nino-like conditions in the Pacific during the Late Pleistocene: a 43 ka noble gas
886 record from California groundwaters. *Quaternary Science Reviews*, *28*(23–24), 2465–
887 2473. https://doi.org/10.1016/J.QUASCIREV.2009.05.008
888 Lachniet, M., Asmerom, Y., Polyak, V., & Denniston, R. (2017). Arctic cryosphere and
889 Milankovitch forcing of Great Basin paleoclimate. *Scientific Reports 2017 7:1*, *7*(1), 1–
890 10. https://doi.org/10.1038/s41598-017-13279-2
891 Lachniet, M. S. (2016). A Speleothem Record of Great Basin Paleoclimate: The Leviathan
892 Chronology, Nevada. In *Developments in Earth Surface Processes* (Vol. 20, pp. 551–
893 569). Elsevier B.V. https://doi.org/10.1016/B978-0-444-63590-7.00020-2
894 Lachniet, Matthew S., Denniston, R. F., Asmerom, Y., & Polyak, V. J. (2014). Orbital control
895 of western North America atmospheric circulation and climate over two glacial cycles.
896 *Nature Communications*, *5*(1), 3805. https://doi.org/10.1038/ncomms4805
897 Laskar, J., Robutel, P., Joutel, F., Gastineau, M., Correia, A. C. M., & Levrard, B. (2004). A
898 long-term numerical solution for the insolation quantities of the Earth. *Astronomy &*
899 *Astrophysics*, *428*(1), 261–285. https://doi.org/10.1051/0004-6361:20041335
900 Lin, J. C., Broecker, W. S., Hemming, S. R., Hajdas, I., Anderson, R. F., Smith, G. I., et al.
901 (1998). A Reassessment of U-Th and 14C Ages for Late-Glacial High-Frequency
902 Hydrological Events at Searles Lake, California. *Quaternary Research*, *49*, 11–23.

https://doi.org/10.1006/qres.1997.1949

Lisiecki, L. E., & Raymo, M. E. (2005). A Pliocene-Pleistocene stack of 57 globally distributed benthic δ18 O records. *Paleoceanography*, *20*(1), n/a-n/a. https://doi.org/10.1029/2004PA001071

Litwin, R. J., Smoot, J. P., Durika, N. J., & Smith, G. I. (1999). Calibrating Late Quaternary terrestrial climate signals: Radiometrically dated pollen evidence from the southern Sierra Nevada, USA. *Quaternary Science Reviews*. https://doi.org/10.1016/S0277-3791(98)00111-5

Loomis, S. E., Russell, J. M., Heureux, A. M., D'Andrea, W. J., & Sinninghe Damsté, J. S. (2014). Seasonal variability of branched glycerol dialkyl glycerol tetraethers (brGDGTs) in a temperate lake system. *Geochimica et Cosmochimica Acta*, *144*, 173–187. https://doi.org/10.1016/j.gca.2014.08.027

Lüthi, D., Le Floch, M., Bereiter, B., Blunier, T., Barnola, J.-M., Siegenthaler, U., et al. (2008). High-resolution carbon dioxide concentration record 650,000–800,000 years before present. *Nature*, *453*(7193), 379–382. https://doi.org/10.1038/nature06949

Lyle, M., Heusser, L., Ravelo, C., Andreasen, D., Olivarez Lyle, A., & Diffenbaugh, N. (2010). Pleistocene water cycle and eastern boundary current processes along the California continental margin. *Paleoceanography*, *25*(4). https://doi.org/10.1029/2009PA001836

Martínez-Sosa, P., Tierney, J. E., Stefanescu, I. C., Dearing Crampton-Flood, E., Shuman, B. N., & Routson, C. (2021). A global Bayesian temperature calibration for lacustrine brGDGTs. *Geochimica et Cosmochimica Acta*, *305*, 87–105. https://doi.org/10.1016/J.GCA.2021.04.038

McGee, D., Moreno-Chamarro, E., Marshall, J., & Galbraith, E. D. (2018). Western U.S. lake expansions during Heinrich stadials linked to Pacific Hadley circulation. *Science Advances*, *4*(11), eaav0118. https://doi.org/10.1126/sciadv.aav0118

McGee, David. (2020, January 3). Glacial-Interglacial Precipitation Changes. *Annual Review of Marine Science*. Annual Reviews. https://doi.org/10.1146/annurev-marine-010419-010859

Moore, J. G., & Moring, B. C. (2013). Rangewide glaciation in the Sierra Nevada, California. *Geosphere*, *9*(6), 1804–1818. https://doi.org/10.1130/GES00891.1

Moseley, G. E., Edwards, R. L., Wendt, K. A., Cheng, H., Dublyansky, Y., Lu, Y., et al. (2016). Reconciliation of the Devils Hole climate record with orbital forcing. *Science (New York, N.Y.)*, *351*(6269), 165–8. https://doi.org/10.1126/science.aad4132

Olson, K. J., & Lowenstein, T. K. (2021). Searles Lake evaporite sequences: Indicators of late Pleistocene/Holocene lake temperatures, brine evolution, and pCO2. *GSA Bulletin*. https://doi.org/10.1130/B35857.1

Oster, J. L., Ibarra, D. E., Winnick, M. J., & Maher, K. (2015). Steering of westerly storms over western North America at the Last Glacial Maximum. *Nature Geoscience*, *8*(3), 201–205. https://doi.org/10.1038/ngeo2365

Pancost, R. D., Hopmans, E. C., & Sinninghe Damsté, J. S. (2001). Archaeal lipids in Mediterranean cold seeps: molecular proxies for anaerobic methane oxidation. *Geochimica et Cosmochimica Acta*, *65*(10), 1611–1627. https://doi.org/10.1016/S0016-7037(00)00562-7

Patten, D. T., Rouse, L., & Stromberg, J. C. (2008). Isolated spring wetlands in the Great Basin and Mojave deserts, USA: Potential response of vegetation to groundwater

withdrawal. *Environmental Management*, *41*(3), 398–413. https://doi.org/10.1007/S00267-007-9035-9

Peaple, M. D., Tierney, J. E., McGee, D., Lowenstein, T. K., Bhattacharya, T., & Feakins, S. J. (2021). Identifying plant wax inputs in lake sediments using machine learning. *Organic Geochemistry*, *156*, 104222. https://doi.org/10.1016/J.ORGGEOCHEM.2021.104222

Pierce, D. W., Cayan, D. R., Das, T., Maurer, E. P., Miller, N. L., Bao, Y., et al. (2013). The Key Role of Heavy Precipitation Events in Climate Model Disagreements of Future Annual Precipitation Changes in California. *Journal of Climate*, *26*(16), 5879–5896. https://doi.org/10.1175/JCLI-D-12-00766.1

Reheis, M. C., Stine, S., & Sarna-Wojcicki, A. M. (2002). Drainage reversals in Mono Basin during the late Pliocene and Pleistocene. *Geological Society of America Bulletin*, *114*(8), 991–1006.

Rimmer, A., Gal, G., Opher, T., Lechinsky, Y., & Yacobi, Y. Z. (2011). Mechanisms of long-term variations in the thermal structure of a warm lake. *Limnology and Oceanography*, *56*(3), 974–988. https://doi.org/10.4319/LO.2011.56.3.0974

Roberts, S. M., & Spencer, R. J. (1998). A desert responds to Pleistocene climate change: Saline lacustrine sediments, Death Valley, California, USA. In *Quaternary Deserts and Climatic Change* (pp. 357–370). CRC Press. https://doi.org/10.1201/9781003077862-37

Russell, J. M., Hopmans, E. C., Loomis, S. E., Liang, J., & Sinninghe Damsté, J. S. (2018). Distributions of 5- and 6-methyl branched glycerol dialkyl glycerol tetraethers (brGDGTs) in East African lake sediment: Effects of temperature, pH, and new lacustrine paleotemperature calibrations. *Organic Geochemistry*, *117*, 56–69. https://doi.org/10.1016/J.ORGGEOCHEM.2017.12.003

Sachse, D., Billault, I., Bowen, G. J., Chikaraishi, Y., Dawson, T. E., Feakins, S. J., et al. (2012). Molecular Paleohydrology: Interpreting the Hydrogen-Isotopic Composition of Lipid Biomarkers from Photosynthesizing Organisms, *40*(1). https://doi.org/10.1146/annurev-earth-042711-105535

Schouten, S., Wakeham, S. G., & Damsté, J. S. S. (2001). Evidence for anaerobic methane oxidation by archaea in euxinic waters of the Black Sea. *Organic Geochemistry*, *32*(10), 1277–1281. https://doi.org/10.1016/S0146-6380(01)00110-3

Schouten, S., Hopmans, E. C., Schefuß, E., & Sinninghe Damsté, J. S. (2002). Distributional veriations in marine crenarchaeol membrane lipids: a new tool for reconstructing ancient sea water temperatures? *Earth and Planetary Science Letters*, *204*, 265–274. https://doi.org/10.1016/S0012-821X(03)00193-6

Schouten, S., Hopmans, E. C., & Sinninghe Damsté, J. S. (2013). The organic geochemistry of glycerol dialkyl glycerol tetraether lipids: A review. *Organic Geochemistry*, *54*, 19–61. https://doi.org/10.1016/J.ORGGEOCHEM.2012.09.006

Seltzer, A. M., Ng, J., Aeschbach, W., Kipfer, R., Kulongoski, J. T., Severinghaus, J. P., & Stute, M. (2021). Widespread six degrees Celsius cooling on land during the Last Glacial Maximum. *Nature*, *593*(7858), 228–232. https://doi.org/10.1038/S41586-021-03467-6

Sinninghe Damsté, J. S., Schouten, S., Hopmans, E. C., Van Duin, A. C. T., & Geenevasen, J. A. J. (2002). Crenarchaeol. *Journal of Lipid Research*, *43*(10), 1641–1651. https://doi.org/10.1194/JLR.M200148-JLR200

Sinninghe Damsté, J. S., Ossebaar, J., Schouten, S., & Verschuren, D. (2012). Distribution of

tetraether lipids in the 25-ka sedimentary record of Lake Challa: extracting reliable TEX86 and MBT/CBT palaeotemperatures from an equatorial African lake. *Quaternary Science Reviews*, *50*, 43–54. https://doi.org/10.1016/J.QUASCIREV.2012.07.001

Sinninghe Damsté, J. S., Rijpstra, W. I. C., Hopmans, E. C., Jung, M. Y., Kim, J. G., Rhee, S. K., et al. (2012). Intact polar and core glycerol dibiphytanyl glycerol tetraether lipids of group I.1a and I.1b Thaumarchaeota in soil. *Applied and Environmental Microbiology*, *78*(19), 6866–6874. https://doi.org/10.1128/AEM.01681-12/ASSET/7E48339A-F904-4F5F-9251-4652603B0C1C/ASSETS/GRAPHIC/ZAM9991036760003.JPEG

Smith, G. I. (2009). Late Cenozoic geology and lacustrine history of Searles Valley, inyo and San Bernardino counties, California. *US Geological Survey Professional Paper*. https://doi.org/10.3133/pp1727

Smith, G. I., Barczak, V. J., Moulton, G. F., & Liddicoat, J. C. (1983). *Core KM-3, a surface-to-bedrock record of late Cenozoic sedimentation in Searles Valley, California*. *Professional Paper*. https://doi.org/10.3133/PP1256

Tabor, C., Lofverstrom, M., Oster, J., Wortham, B., de Wet, C., Montañez, I., et al. (2021). A mechanistic understanding of oxygen isotopic changes in the Western United States at the Last Glacial Maximum. *Quaternary Science Reviews*, *274*, 107255. https://doi.org/10.1016/J.QUASCIREV.2021.107255

Thompson, R. S., & Anderson, K. H. (2000). Biomes of western North America at 18,000, 6000 and 0 14C yr BP reconstructed from pollen and packrat midden data. *Journal of Biogeography*, *27*(3), 555–584. https://doi.org/10.1046/J.1365-2699.2000.00427.X

Tierney, J. E., Mayes, M. T., Meyer, N., Johnson, C., Swarzenski, P. W., Cohen, A. S., & Russell, J. M. (2010). Late-twentieth-century warming in Lake Tanganyika unprecedented since AD 500. *Nature Geoscience 2010 3:6*, *3*(6), 422–425. https://doi.org/10.1038/ngeo865

Verschuren, D., Sinninghe Damsté, J. S., Moernaut, J., Kristen, I., Blaauw, M., Fagot, M., & Haug, G. H. (2009). Half-precessional dynamics of monsoon rainfall near the East African Equator. *Nature 2009 462:7273*, *462*(7273), 637–641. https://doi.org/10.1038/nature08520

Wang, H., Liu, W., Zhang, C. L., Jiang, H., Dong, H., Lu, H., & Wang, J. (2013). Assessing the ratio of archaeol to caldarchaeol as a salinity proxy in highland lakes on the northeastern Qinghai–Tibetan Plateau. *Organic Geochemistry*, *54*, 69–77. https://doi.org/10.1016/J.ORGGEOCHEM.2012.09.011

Wang, H., Liu, W., He, Y., Zhou, A., Zhao, H., Liu, H., et al. (2021). Salinity-controlled isomerization of lacustrine brGDGTs impacts the associated MBT5ME' terrestrial temperature index. *Geochimica et Cosmochimica Acta*, *305*, 33–48. https://doi.org/10.1016/J.GCA.2021.05.004

Wang, Z., Zhang, F., Cao, Y., Hu, J., Wang, H., Lu, H., et al. (2022). Linking sedimentary and speleothem precipitation isotope proxy records to improve lacustrine and marine 14C chronologies. *Quaternary Science Reviews*, *282*, 107444. https://doi.org/10.1016/J.QUASCIREV.2022.107444

Wendt, K. A., Dublyansky, Y. V., Moseley, G. E., Edwards, R. L., Cheng, H., & Spötl, C. (2018). Moisture availability in the southwest United States over the last three glacial-interglacial cycles. *Science Advances*, *4*(10), eaau1375.

Western Regional Climate Center. (2022). US COOP Station Map. Retrieved October 31, 2018, from https://wrcc.dri.edu/coopmap/

Willson, C. J., Manos, P. S., & Jackson, R. B. (2008). Hydraulic traits are influenced by phylogenetic history in the drought-resistant, invasive genus Juniperus (Cupressaceae). *American Journal of Botany*, *95*(3), 299–314. https://doi.org/10.3732/AJB.95.3.299

Winograd, I. J., Coplen, T. B., Landwehr, J. M., Riggs, A. C., Ludwig, K. R., Szabo, B. J., et al. (1992). Continuous 500,000-year climate record from vein calcite in Devils Hole, Nevada. *Science*, *258*(5080), 255–260. https://doi.org/10.1126/science.258.5080.255

Wood, G. D. (2000). Pollen analysis of death valley sediments deposited between 166 and 114 ka. *Palynology*, *24*(1), 49–61. https://doi.org/10.1080/01916122.2000.9989537

Woolfenden, W. B. (2003). A 180,000-year pollen record from Owens Lake, CA: Terrestrial vegetation change on orbital sales. *Quaternary Research*, *59*(3), 430–444. https://doi.org/10.1016/S0033-5894(03)00033-4

References from the supporting information

Aichner, B., Herzschuh, U., & Wilkes, H. (2010). Influence of aquatic macrophytes on the stable carbon isotopic signatures of sedimentary organic matter in lakes on the Tibetan Plateau. *Organic Geochemistry*, *41*(7), 706–718. https://doi.org/10.1016/j.orggeochem.2010.02.002

Aichner, B., Hilt, S., Périllon, C., Gillefalk, M., & Sachse, D. (2017). Biosynthetic hydrogen isotopic fractionation factors during lipid synthesis in submerged aquatic macrophytes: Effect of groundwater discharge and salinity. *Organic Geochemistry*, *113*, 10–16. https://doi.org/10.1016/J.ORGGEOCHEM.2017.07.021

Bi, X., Sheng, G., Liu, X., Li, C., & Fu, J. (2005). Molecular and carbon and hydrogen isotopic composition of n-alkanes in plant leaf waxes. *Organic Geochemistry*, *36*(10), 1405–1417. https://doi.org/10.1016/J.ORGGEOCHEM.2005.06.001

Czop, M., Motyka, J., Sracek, O., & Szuwarzyński, M. (2011). Geochemistry of the hyperalkaline Gorka pit lake (pH>13) in the Chrzanow region, southern Poland. *Water, Air, and Soil Pollution*, *214*(1–4), 423–434. https://doi.org/10.1007/s11270-010-0433-x

Dearing Crampton-Flood, E., Tierney, J. E., Peterse, F., Kirkels, F. M. S. A., & Sinninghe Damsté, J. S. (2020). BayMBT: A Bayesian calibration model for branched glycerol dialkyl glycerol tetraethers in soils and peats. *Geochimica et Cosmochimica Acta*, *268*, 142–159. https://doi.org/10.1016/j.gca.2019.09.043

Diefendorf, A. F., Leslie, A. B., & Wing, S. L. (2015). Leaf wax composition and carbon isotopes vary among major conifer groups. *Geochimica et Cosmochimica Acta*, *170*, 145–156. https://doi.org/10.1016/j.gca.2015.08.018

Feakins, S. J. (2013). Pollen-corrected leaf wax D/H reconstructions of northeast African hydrological changes during the late Miocene. *Palaeogeography, Palaeoclimatology, Palaeoecology*, *374*, 62–71. https://doi.org/10.1016/J.PALAEO.2013.01.004

Feakins, S. J., & Sessions, A. L. (2010). Controls on the D/H ratios of plant leaf waxes in an arid ecosystem. *Geochimica et Cosmochimica Acta*, *74*(7), 2128–2141. https://doi.org/10.1016/J.GCA.2010.01.016

Fornace, K. L., Whitney, B. S., Galy, V., Hughen, K. A., & Mayle, F. E. (2016). Late Quaternary environmental change in the interior South American tropics: new insight from leaf wax stable isotopes. *Earth and Planetary Science Letters*, *438*, 75–85. https://doi.org/10.1016/J.EPSL.2016.01.007

Freimuth, E. J., Diefendorf, A. F., & Lowell, T. V. (2017). Hydrogen isotopes of n-alkanes and n-alkanoic acids as tracers of precipitation in a temperate forest and implications for paleorecords. *Geochimica et Cosmochimica Acta*, *206*, 166–183. https://doi.org/10.1016/J.GCA.2017.02.027

Hay, R. L., Guldman, S. G., Matthews, J. C., Lander, R. H., Duffin, M. E., & Kyser, T. K. (1991). Clay mineral diagenesis in core KM-3 of Searles Lake, California. *Clays and Clay Minerals*, *39*(1), 84–96. https://doi.org/10.1346/CCMN.1991.0390111

Inglis, G. N., Carmichael, M. J., Farnsworth, A., Lunt, D. J., & Pancost, R. D. (2020). A long-term, high-latitude record of Eocene hydrological change in the Greenland region. *Palaeogeography, Palaeoclimatology, Palaeoecology*, *537*, 109378. https://doi.org/10.1016/J.PALAEO.2019.109378

Krull, E., Sachse, D., Mügler, I., Thiele, A., & Gleixner, G. (2006). Compound-specific δ13C and δ2H analyses of plant and soil organic matter: A preliminary assessment of the effects of vegetation change on ecosystem hydrology. *Soil Biology and Biochemistry*, *38*(11), 3211–3221. https://doi.org/10.1016/J.SOILBIO.2006.04.008

Lisiecki, L. E., & Raymo, M. E. (2005). A Pliocene-Pleistocene stack of 57 globally distributed benthic δ18 O records. *Paleoceanography*, *20*(1), n/a-n/a. https://doi.org/10.1029/2004PA001071

Litwin, R. J., Smoot, J. P., Durika, N. J., & Smith, G. I. (1999). Calibrating Late Quaternary terrestrial climate signals: Radiometrically dated pollen evidence from the southern Sierra Nevada, USA. *Quaternary Science Reviews*. https://doi.org/10.1016/S0277-3791(98)00111-5

Liu, W., Yang, H., & Li, L. (2006). Hydrogen isotopic compositions of n-alkanes from terrestrial plants correlate with their ecological life forms. *GLOB AL CHANGE AND CONSERVATION ECOLOGY*, *150*, 330–338. https://doi.org/10.1007/s00442-006-0494-0

Makou, M., Eglinton, T., McIntyre, C., Montluçon, D., Antheaume, I., & Grossi, V. (2018). Plant Wax n -Alkane and n -Alkanoic Acid Signatures Overprinted by Microbial Contributions and Old Carbon in Meromictic Lake Sediments. *Geophysical Research Letters*, *45*(2), 1049–1057. https://doi.org/10.1002/2017GL076211

Martínez-Sosa, P., Tierney, J. E., Stefanescu, I. C., Dearing Crampton-Flood, E., Shuman, B. N., & Routson, C. (2021). A global Bayesian temperature calibration for lacustrine brGDGTs. *Geochimica et Cosmochimica Acta*, *305*, 87–105. https://doi.org/10.1016/J.GCA.2021.04.038

McCallister, S. L., & Del Giorgio, P. A. (2008). Direct measurement of the δ13C signature of carbon respired by bacteria in lakes: Linkages to potential carbon sources, ecosystem baseline metabolism, and CO2 fluxes. *Limnology and Oceanography*, *53*(4), 1204–1216. https://doi.org/10.4319/lo.2008.53.4.1204

Nobel, P. S., & Bobich, E. G. (2002). Initial Net CO2 Uptake Responses and Root Growth for a CAM Community Placed in a Closed Environment. *Annals of Botany*, *90*(5), 593–598. https://doi.org/10.1093/AOB/MCF229

Peaple, M. D., Tierney, J. E., McGee, D., Lowenstein, T. K., Bhattacharya, T., & Feakins, S. J. (2021). Identifying plant wax inputs in lake sediments using machine learning. *Organic Geochemistry*, *156*, 104222. https://doi.org/10.1016/J.ORGGEOCHEM.2021.104222

Pennington, W. (1979). The origin of pollen in lakes sedimetns: an enclosed lake compared with one recieiving inflow stream. *New Phytologist*, *83*(1), 189–213. https://doi.org/10.1111/j.1469-8137.1979.tb00741.x

Russell, J. M., Hopmans, E. C., Loomis, S. E., Liang, J., & Sinninghe Damsté, J. S. (2018). Distributions of 5- and 6-methyl branched glycerol dialkyl glycerol tetraethers (brGDGTs) in East African lake sediment: Effects of temperature, pH, and new lacustrine paleotemperature calibrations. *Organic Geochemistry*, *117*, 56–69. https://doi.org/10.1016/J.ORGGEOCHEM.2017.12.003

Sachse, D., Billault, I., Bowen, G. J., Chikaraishi, Y., Dawson, T. E., Feakins, S. J., et al. (2012). Molecular Paleohydrology: Interpreting the Hydrogen-Isotopic Composition of Lipid Biomarkers from Photosynthesizing Organisms, *40*(1). https://doi.org/10.1146/annurev-earth-042711-105535

Tamalavage, A. E., van Hengstum, P. J., Louchouarn, P., Fall, P. L., Donnelly, J. P., Albury, N. A., et al. (2020). Plant wax evidence for precipitation and vegetation change from a coastal sinkhole lake in the Bahamas spanning the last 3000 years. *Organic Geochemistry*, *150*, 104120. https://doi.org/10.1016/J.ORGGEOCHEM.2020.104120

Tipple, B. J., & Pagani, M. (2010). A 35 Myr North American leaf-wax compound-specific carbon and hydrogen isotope record: Implications for C4 grasslands and hydrologic cycle dynamics. *Earth and Planetary Science Letters*, *299*(1–2), 250–262. https://doi.org/10.1016/J.EPSL.2010.09.006

Tipple, B. J., & Pagani, M. (2013). Environmental control on eastern broadleaf forest speciesâ€™ leaf wax distributions and D/H ratios. *Geochimica et Cosmochimica Acta*, *111*, 64–77. https://doi.org/10.1016/j.gca.2012.10.042

Turich, C., & Freeman, K. H. (2011). Archaeal lipids record paleosalinity in hypersaline systems. *Organic Geochemistry*, *42*(9), 1147–1157. https://doi.org/10.1016/J.ORGGEOCHEM.2011.06.002

Williams, D. G., & Ehleringer, J. R. (2000). Intra- and Interspecific Variation for Summer Precipitation Use in Pinyon-Juniper Woodlands. *Ecological Monographs*, *70*(4), 517. https://doi.org/10.2307/2657185

Windler, G., Tierney, J. E., Zhu, J., & Poulsen, C. J. (2020). Unraveling Glacial Hydroclimate in the Indo-Pacific Warm Pool: Perspectives From Water Isotopes. *Paleoceanography and Paleoclimatology*, *35*(12), e2020PA003985. https://doi.org/10.1029/2020PA003985

Woolfenden, W. B. (2003). A 180,000-year pollen record from Owens Lake, CA: Terrestrial vegetation change on orbital sales. *Quaternary Research*, *59*(3), 430–444. https://doi.org/10.1016/S0033-5894(03)00033-4

Xia, L., Cao, J., Stüeken, E. E., Zhi, D., Wang, T., & Li, W. (2020). Unsynchronized evolution of salinity and pH of a Permian alkaline lake influenced by hydrothermal fluids: A multi-proxy geochemical study. *Chemical Geology*, *541*, 119581. https://doi.org/10.1016/J.CHEMGEO.2020.119581

Yu, K., D'odorico, P., Collins, S. L., Carr, D., Porporato, A., Anderegg, W. R. L., et al. (2019). The competitive advantage of a constitutive CAM species over a C4 grass species under drought and CO2 enrichment. *Ecosphere*, *10*(5), e02721. https://doi.org/10.1002/ECS2.2721